



THE UNIVERSITY OF QUEENSLAND
A U S T R A L I A

A Multi-scale Approach to the Detection of the Isolated Spectrum of Transfer Operators

Hayden Reece Hohns

Under the supervision of
Cecilia González-Tokman

*A Thesis Submitted in Partial Fulfilment of the
Requirements of the Bachelor of Science with Honours
Degree*

School of Mathematics and Physics
University of Queensland
Australia
November 7, 2016

Abstract

Invariant sets and transfer operators are a central focus in the study of ergodic theory due to their broad applications to science and engineering as well as purely theoretical exploits. However, with a slight perturbation — a more realistic model of applied problems, the notion of “almost-invariance” greatly influences the complexity of the dynamics. Transfer operators are used to study a large class of dynamical systems, including discrete time maps and continuous flows (i.e., differential equations and Markov chains). Both theoretical and numerical literature take advantage of operator theory and functional analysis to better understand these operators. For the approach we pursue in this work, it is crucial to ensure that on whichever function space one is studying these operators, that said operator is quasicompact — that is, one can split up the spectrum into a discrete and continuous part. This is important as it allows one to characterise the slowly mixing regions of a dynamical system. In particular, the spectrum of such operators can be relatively complex and determining the isolated spectrum, used along with the corresponding eigenspaces to investigate invariant measures and almost-invariant structures is not a trivial task. In 2014, Froyland, González-Tokman, and Quas used harmonic analysis ideas to smooth eigenvectors and determine the number of isolated eigenvectors, corresponding to almost-invariant sets. In this work, a numerical method based on an alternative wavelet theory approach is developed, and its results are compared with the outcome of Froyland, González-Tokman, and Quas. The underlying theory for this approach is summarised with code to run in MATLAB. This algorithm can be readily used in order to determine the number of slowly mixing regions of a dynamical system (e.g., eddies in a fluid flow simulation). Future development and open problems relating to the spectrum and stability of transfer operators and their numerical methods are also discussed.

Acknowledgements

First, I would like to express my sincerest appreciation to my supervisor Cecilia González-Tokman for her support over the year. Without her supervision, this project almost surely (see what I did there!) would not have come to fruition. Her expertise in the field eased me into the technical areas of dynamical systems/ergodic theory, and was very flexible to my own particular skill set, giving me much freedom throughout this year. Furthermore, we also started the first run of measurable dynamics and ergodic theory seminars this year. Without her, these also would not have come to fruition. I hope that these continue well into the future, as they help bring the mathematics community closer and provide a glimpse into higher level mathematics.

In addition to my supervisor, many other UQ SMP staff deserve to be mentioned. Special thanks go to Doctor Yoni Nazarathy and Professor Dirk Kroese, our coordinators for the UQ Maths Honours Program, and Doctor Thomas Taimre, who provided a great deal of advice in both academic writing and life skills. Thomas also helped facilitate the advanced numerical analysis (reading) course in the second semester which was a lot of fun and I learned a great deal about modern scientific computing. I am also appreciative of the opportunities to both attend and present at various seminars this year, including weekly visits to the analysis, dynamics, and probability seminars. These not only provided me with valuable opportunities to improve various skills, but gain a wider perspective and appreciation of different fields and ideas in mathematics.

I must also express my gratitude towards my friends and fellow UQ Maths Honours students. They have been particularly kind and outgoing towards me. More specifically, I would like to thank (in no particular order) Liam Hodgkinson, Marielle Ong, Aiden Suter, Matthew Habermann, Luke Mitchelson, Anna Kervison, Nathan D'Addio, Thomas Anderson, Timothy Buttsworth, Kyle McLaren, Rixon Crane, Alexandra Gloria, Anthea Le, and Adam Walsh. They are all very kind and bright people, and I wish them nothing but the best. A special mention goes to my friend Daniel Defries, a friend who has stuck by me for more than half of my life (which is an achievement in itself – to put up with me for that long!).

Last and certainly not least, I would like to thank my family for an approximately infinite number of things (although the stand out would certainly be their patience with me).

Contents

1	Introduction	2
1.1	Notation	4
2	Background Review	5
2.1	Dynamical Systems and Ergodic Theory	5
2.2	The Frobenius–Perron and Koopman Operators	8
2.2.1	Semigroups for Transfer Operators	13
2.2.2	Establishing the Relationship Between the Frobenius–Perron and Koopman Operators	17
2.3	Ulam’s Method	19
2.3.1	History and Theory	19
2.3.2	The Markov Partition and Other Considerations	24
2.4	Literature Review	26
2.4.1	The Dellnitz–Froyland Ansatz	26
2.4.2	Detecting Isolated Spectrum of Transfer and Composition Operators with Harmonic Analysis	29
3	A Wavelet Approach to the Spectrum of Transfer Operators	35
3.1	Wavelet Theory	35
3.2	The Algorithm	37
3.2.1	Numerical Experiments	38
4	Discussion and Conclusions	46
A	MATLAB Code	48
A.1	Ulam’s method	48
A.2	Wavelet threshold for fractional Sobolev norm	50
A.3	Quadruple-gyre Code	53

List of Figures and Tables

2.1	Visual representation of Ulam's method. Note that it is important to sample the same number of points from each box in order to capture all features of the dynamical system at a given resolution.	21
2.2	The original double-gyre system at the initial time $t = 0$	22
2.3	Approximation to the eigenfunctions of the transfer operator for the double-gyre.	23
2.4	A comparison of the computational complexity of the Haar basis and the standard basis for Ulam's method.	23
2.5	Demonstration of the Lipschitz continuity.	25
2.6	Spectrum of a stochastic matrix in the complex plane. The second eigenvalue, λ_2 describes the geometric convergence of the power method.	26
2.7	Graph of T_t for $t = 31/8$	27
2.8	The map given by equation (2.4.2) with parameters $\varepsilon = 0$ and $\delta = 0$	29
2.9	A comparison of the left and right eigenvectors of the dynamical system given by (2.4.2).	31
2.10	A comparison of the unperturbed and perturbed spectrum of the Koopman operator.	32
3.1	A visual demonstration of the multiscale/wavelet analysis. Here, one may think of scale related to "frequency" in the Fourier domain.	39
3.2	The Morlet/Gabor wavelet, $\psi(x) = \psi_{1,0}(x) = e^{-x^2/2} \cos(5x)$	40
3.3	The Mexican hat wavelet, $\psi(x) = C(1 - x^2)e^{-x^2/2}$	41
3.4	A plot of the eigenvectors and their fractional Sobolev norms under the six different wavelets and the Fourier basis.	42
3.5	Left and right eigenvector norms for $\varepsilon = 0.1$ and $\delta = 0.25$	43

Chapter 1

Introduction

Measurable dynamics, otherwise known as ergodic theory, was first developed through the theory of dynamical systems in conjunction with a sub-field of theoretical physics known as statistical mechanics. The theory of dynamical systems arguably begins with the work of Poincaré (1854–1912), who identified the the intrinsic relationship between the theory of differential equations and differential geometry. Much of the work by Poincaré was motivated by the three-body problem, a topic that was of great interest to mathematicians and physicists alike who were studying the motion of planets. Poincaré was also the first to discover a chaotic system of differential equations.

Statistical mechanics arose when the chaos observed in Newtonian dynamics proved too difficult to work with, and a probabilistic approach was developed. A central part of statistical mechanics was developed by L. Boltzmann (1844 – 1906), who conjectured in 1872 the “ergodic hypothesis”, which loosely translates to “the space and time averages are equal”. This was later formalised by G. D. Birkhoff (1884 – 1944) who discovered one of the most notable results in ergodic theory, which is now known as the “Birkhoff Ergodic Theorem” (published in 1931). Numerous ergodic theorems are now known throughout the literature, such as von Neumann and Oseledec’s ergodic theorem.

Since then, the field of ergodic theory has grown, the result of Birkhoff proving to be instrumental in the development and applications of many fields of mathematics, such as dynamics, group theory, probability theory, number theory, differential geometry, and functional analysis. S. Ulam (1909 – 1984) was the first to propose what would arguably become the most widely used numerical method for computational ergodic theory in 1960. This method can be formulated as a special case of the Galerkin method, a typical approach used for solving partial differential equations via the finite element method. However, until recently, ergodic theory had remained a largely theoretical and esoteric field of mathematics. It was not until the 1990’s with the recent advent of accessible high-performance computing technology that it became feasible to discretely represent and simulate a transfer operator in a computer. With the rapid improvements to computing technologies, computational measurable dynamics has begun to flourish both theoretically and heuristically.

Theoretical and numerical methods used for the analysis of long-term behaviour of a dynamical system typically employ geometric or probabilistic techniques. Geometric methods rely on the qualitative theory of differential equations — that is, fixed-point analysis, periodic orbits, and invariant manifolds. In particular, invariant manifolds and periodic orbits act as transport barriers since trajectories cannot cross the manifolds transversally. Probabilistic or ensemble methods look at the distribution of points after simulating long trajectories. If the system possesses an invariant density, then these methods may assist in partitioning the state space into almost-invariant sets. These

represent regions in which the state space is almost dynamically disconnected.

One of the most common approaches used in computational dynamics are commonly referred to as the “ensemble perspective” or “set oriented methods” in the literature. This perspective is reminiscent of the duality between Lagrangian and Eulerian dynamics. The Lagrangian approach is much like following the trajectory of a single ordinary differential equation, a fluid particle has a set of assigned properties such as density and velocity. This approach is typically quite expensive in terms of numerical computation. On the other hand, the Eulerian specification describes the fluid as a whole, and how it evolves over time, much like the aforementioned set-oriented methods.

A particular operator that is central to the study of ergodic theory is called the Frobenius–Perron (or transfer) operator, and when defined on an appropriate function space, is also studied through its adjoint, known as the Koopman (or composition) operator. These operators describe a natural “push-forward” and “pull-back” (respectively) on a given dynamical system. A problem unique to computational mathematics is that different algorithms for computing the same quantity can yield vastly different results due to stability (e.g., Gram–Schmidt versus Modified Gram–Schmidt). In a similar manner, computational ergodic theory is still in the phase of developing more computer adapted algorithms, as opposed to directly applying the results of various theorems.

Both the Frobenius–Perron and Koopman operators have been used to study the global behaviour of a dynamical system but have significantly different computational methods associated with them. The primary approach to approximating the Frobenius–Perron operator is via Ulam’s method and is similar to the Galerkin method commonly found in finite element analysis. Ulam’s method typically requires a large number of initial conditions but a short simulation time. However, due to the curse of dimensionality, this method is unsuitable for high dimensional applications. Despite the duality between the two operators, techniques and consequences of them are not mutually disjoint from each other. Other methods exist specifically for the Koopman operator but these also suffer from similar problems to Ulam’s method. Resolving these computational complexity issues are still open problems in the field. Indeed, the Frobenius–Perron and Koopman operators are infinite-dimensional linear operators, capable of capturing the fully non-linear dynamics of a given system, but the algorithms used to approximate these operators are often direct numerical schemes of recently proved theorems.

Computational measurable dynamics is at a stage where it is soon ready to transfer from an academic setting to industrial practice (e.g., computational fluid dynamics or meteorology), but in order for its strengths to be realised, more effort is required in developing algorithmic techniques to overcome complexity issues (such as the aforementioned curse of dimensionality).

The aim of this thesis is twofold:

- (i) To provide a cohesive exposition of some aspects of pure and computational ergodic theory, drawing upon the rich mathematical ideas present in the literature; and
- (ii) To investigate almost-invariant components of dynamical systems and provide an answer to the more recent problem of detecting the number of elements in the isolated spectrum of transfer operators.

There is no assumed background on transfer operators, ergodic theory, or dynamical systems. However, the reader is expected to be comfortable with elements of differential equations, functional/harmonic analysis, linear algebra, measure theory, introductory scientific computing, and probability.

1.1 Notation

Before proceeding, notation will be as follows. For a number system such as \mathbb{R} or \mathbb{Z} , a $+$ in the subscript will denote the restriction to the set of non-negative numbers, i.e., $\mathbb{R}_+ = \{x \in \mathbb{R} : x \geq 0\}$ and $\mathbb{Z}_+ = \{n \in \mathbb{Z} : n \geq 0\}$. Calligraphic mathematical letters will denote mathematical operators unless otherwise stated, and in particular, \mathcal{P} and \mathcal{K} will denote the Frobenius–Perron and Koopman operators respectively, later to be defined precisely. In general, the state space \mathbb{X} is a Riemannian manifold or subset of \mathbb{R}^d and \mathbb{B} is an N -cube (i.e., box [2-D] or bin [1-D]). The symbol $\mathbb{1}_S(x)$ denotes the indicator function on the set $S \subset \mathbb{X}$, explicitly given by

$$\mathbb{1}_S(x) = \begin{cases} 1 & \text{if } x \in S, \\ 0 & \text{otherwise.} \end{cases}$$

For the metric space (\mathbb{X}, ϱ) , the diameter of a subset $A \subset \mathbb{X}$, will be denoted by $\text{diam}(A) = \sup\{\varrho(x, y) : x, y \in A\}$. Standard notation seen in harmonic analysis is used unless stated otherwise, for example, $\widehat{f}(\xi)$ will denote the Fourier transform of a function and will take ξ as a variable for Fourier space and otherwise for any other space. Lebesgue spaces are denoted by $L^p(\mathbb{X})$, in which the measure and σ -algebra are clear based on context. A ball of radius r with centre c will be denoted by $B_r(c)$. Functions with k continuous derivatives are denoted by $C^k(\mathbb{X})$ and if the derivative has α -Hölder continuity then it is denoted by e.g., $C^{1+\alpha}(\mathbb{X})$ for continuous derivative with Hölder exponent α .

Chapter 2

Background Review

Although the material contained in this section provides a concise overview of the theory and modern tools used in this thesis, references that expand upon this can be found in [4], [15], and [16]. In particular, the author recommends [16] for theory and both [4] and [15] for numerical methods. The majority of notation is borrowed from [16] in addition to many of the derivations, while the section on spectral properties is taken from [2].

2.1 Dynamical Systems and Ergodic Theory

In general, the motivation for ergodic theory is to describe the behaviour of a map, T_n , or flow, T_t , on a non-empty set \mathbb{X} as $n \rightarrow \infty$ (resp. $t \rightarrow \infty$). Suppose \mathbb{X} is a non-empty set whose elements are acted on by an automorphic transformation, $T : \mathbb{X} \circlearrowright$. Here, \mathbb{X} is called the *state space* and T , which depending on the setting will either be called a *flow*, *semiflow*, or *map*. This nomenclature can be summarised as follows:

- Flow: T_t , $t \in \mathbb{R}$;
- Semi-flow: T_t , $t \in \mathbb{R}_+$;
- Invertible Discrete-time Mapping: T_n , $n \in \mathbb{Z}$;
- Non-invertible Discrete-time Mapping: T_n , $n \in \mathbb{Z}_+$.

Often, one requires some additional structure on the space. In the case of measurable dynamics, one often begins with a triplet $(\mathbb{X}, \mathcal{A}, \mu)$ called a *measure space*, if it satisfies the following axioms:

- (i) \mathbb{X} is a set (e.g., a compact metric space, Riemannian manifold);
- (ii) \mathcal{A} is a σ -algebra, i.e., \mathcal{A} is a collection of subsets of \mathbb{X} (containing the empty set) that are closed under countable unions and complements; and
- (iii) The function $\mu : \mathcal{A} \rightarrow [0, \infty)$ is a measure, i.e., a σ -additive function on \mathcal{A} .

Although it is possible to formulate much of ergodic theory in terms of infinite measure spaces (see [1]), it is much more intuitive to work with a σ -finite measure. Upon normalisation, we call $(\mathbb{X}, \mathcal{A}, \mu)$ a *probability space*. A family of transformations $T_t : \mathbb{R}^d \circlearrowright$ for $t \in \mathbb{R}$ such that $T_0 = \text{Id}$ and the additive group property

$$T_{s+t} = T_s \circ T_t$$

for $s, t \in \mathbb{R}$ holds, then T_t is called a *flow*. If t and s are restricted to \mathbb{R}_+ then $T_t : \mathbb{R}^n \circlearrowleft$ is called a *semiflow*. If time is considered discrete then replacing T_t with T_n and \mathbb{R}^d with \mathbb{Z}^d yields an *invertible map* and once again, restricting to \mathbb{Z}_+^d gives a *non-invertible map*. If the state space is a discrete dynamical system ($n \in \mathbb{Z}_+$), then denote $T_n(x) = T_{n-1} \circ T(x) = T \circ \dots \circ T(x)$ (n times) the n -th composition of T at x with $T_0 = \text{Id}$ (identity). If $T_n(x)$ is invertible, then the ‘‘doubly-infinite’’ sequence $\{T_n(x)\}_{n \in \mathbb{Z}}$ is called the *full orbit* of T while the infinite sequence $\{T_n(x)\}_{n \in \mathbb{Z}_+}$ is called the *forward orbit* of T . The pair (T_t, \mathbb{X}) is called a *dynamical system* (resp. *semidynamical system*) if $T_t : \mathbb{X} \circlearrowleft$ is a family of transformations satisfying¹:

- (i) $T_0(x) = x$ for all $x \in \mathbb{X}$;
- (ii) $T_s(T_t(x)) = T_{s+t}(x)$ for all $x \in \mathbb{X}$ and $s, t \in \mathbb{R}$ (resp. $s, t \in \mathbb{R}_+$); and
- (iii) The mapping $(t, x) \rightarrow T_t(x)$ from $\mathbb{R} \times \mathbb{X}$ (resp. $\mathbb{R}_+ \times \mathbb{X}$) into \mathbb{X} is continuous.

It will be assumed that T is a non-singular transformation — that is, T is called *non-singular* with respect to a given probability space $(\mathbb{X}, \mathcal{A}, \mu)$, then for any $A \in \mathcal{A}$, $\mu(A) = 0$ implies that $\mu(T^{-1}(A)) = 0$. Sometimes it is not strong enough to assume T is non-singular, and thus we may require the property of invariance. More formally, on a measure space $(\mathbb{X}, \mathcal{A}, \mu)$, we call μ an *invariant measure* if for measurable $T : \mathbb{X} \circlearrowleft$ and every measurable $A \in \mathcal{A}$ we have $\mu(T^{-1}(A)) = \mu(A)$. Similarly, we refer to the measure μ as *T -invariant*, or *T preserves μ* , or T is a *measure-preserving transformation*. An analogous definition holds for flows, and although this condition may look restrictive, colloquially, this simply requires that our system is ‘volume-preserving’.

Dynamical systems often exhibit complicated behaviour in fairly novel situations (such as the examples below), and can be misleading to consider a single orbit for a long time. Instead, the ensemble approach suggests to approximate the statistics of the underlying dynamics. This irregularity in structure can be classified into three main cases²: ergodicity, mixing, and exactness.

Definition 2.1.1 (Ergodic, Mixing, Exactness). Let $(\mathbb{X}, \mathcal{A}, \mu)$ be a probability space and $T : \mathbb{X} \circlearrowleft$ be a non-singular transformation. Then we call T *ergodic* if for each invariant set $A \in \mathcal{A}$ we have that $\mu(A) = 0$ or $\mu(A^c) = 0$ — that is, T is ergodic if all invariant sets are trivial subsets of \mathbb{X} . If $T : \mathbb{X} \circlearrowleft$ is also a measure-preserving transformation, then T is:

- (i) *mixing*³ if the following holds

$$\lim_{n \rightarrow \infty} \mu(A \cap T^{-n}(B)) = \mu(A)\mu(B)$$

for all $A, B \in \mathcal{A}$; and

- (ii) *exact* if for $T(A) \in \mathcal{A}$ for each $A \in \mathcal{A}$ and

$$\lim_{n \rightarrow \infty} \mu(T^n(A)) = 1$$

for each $A \in \mathcal{A}$ and $\mu(A) > 0$.

¹Those familiar with Feller processes may recognise the similarity of these axioms with those of a Feller probability semigroup.

²There are more than these three, although they are the main concern in ergodic theory. There are other notions of mixing in probability that are more specific than these.

³Readers who are already familiar with this phenomenon may recognise this more formally as *strong mixing*. There is also a property called *weak mixing* which will not be discussed. We refer the reader to [26].

It can be shown (from the definition) that the exactness of T implies T is also mixing (which is highly non-trivial) and that mixing implies ergodicity (but not the other way around). Intuitively speaking, ergodicity implies that the whole state space is visited under the orbit of dynamical system (this is emphasised in the circle rotation example below).

Before delving into the theory of transfer operators, we will outline some examples that illustrate the types of mathematical objects one may encounter in the theory of measurable dynamics.

Example 2.1.2 (Leaky Bucket). This non-linear ordinary differential equation is an example of a non-reversible autonomous dynamical system (semiflow), defined as

$$\dot{x} = -C\sqrt{|x|}, \quad x(0) = x_0,$$

where C is a positive constant and the dot denotes the derivative with respect to time. This describes the height of water in a bucket with a hole at the bottom and how it changes (with rate C). Besides the trivial solution, $x(t) = 0$ for all t , one can apply separation of variables (two cases for when $x > 0$ and $x < 0$) to determine that

$$x(t) = \begin{cases} +C^2(t-t_1)^2/4 & \text{for } t \leq t_1 \\ 0 & \text{for } t_1 \leq t \leq t_2 \\ -C^2(t-t_2)^2/4 & \text{for } t \geq t_2 \end{cases}$$

is a solution to the leaky bucket differential equation. Note that its solutions do not possess uniqueness.

As was mentioned before, the leaky bucket is an example of a continuous-time dynamical system, or more specifically, a semiflow. We now give an example of a discrete-time dynamical system:

Example 2.1.3 (Angle-Doubling map). Consider the following map on $\mathbb{X} = [0, 1)$, otherwise known as the *angle-doubling map*, given by $T(x) = 2x \bmod 1$. Explicitly, it is written as

$$T(x) = \begin{cases} 2x & 0 \leq x < 1/2 \\ 2x - 1 & 1/2 \leq x < 1. \end{cases}$$

It is an example of a measure preserving transformation that is not invertible since it is everywhere 2-to-1 and cannot be made 1-to-1 by an alteration on a non-measurable set.

Example 2.1.4 (Translations of the circle). Let \mathbb{X} be the circle given by the quotient space, $\mathbb{T} = \mathbb{R} \setminus \mathbb{Z} = [0, 1)$, \mathcal{A} its Borel sets, and μ the Lebesgue measure. The *rotation*, or *translation* of the circle by $\alpha \in \mathbb{X}$ is the transformation $R_\alpha(x) : \mathbb{X} \circlearrowleft$ defined by $R_\alpha(x) = x + \alpha \bmod 1$. One can see that this is measure-preserving ($\mu \circ R_\alpha(x) = \mu$) and is invertible. One can show that $R_\alpha(x)$ is ergodic (using harmonic analysis) if and only if α is irrational.

As one can see, the study of flows and maps, or, continuous-time and discrete-time vary greatly. Section 2.2 aims to highlight these differences.

2.2 The Frobenius–Perron and Koopman Operators

Historically, transfer operators were introduced in the ergodic theory literature when physicists were interested in steady-state behaviour in molecular dynamics [12]. Since then, ergodic theory has enjoyed applications in many areas such as computational fluid dynamics, (deterministic and stochastic) dynamical systems, partial differential equations, and control theory. One theorem that is central to the work in measurable dynamics is based on is the Frobenius–Perron theorem.

Theorem 2.2.1 (Perron–Frobenius). *Suppose $A = [a_{i,j}]$ is an $N \times N$ matrix with strictly non-negative entries ($a_{i,j} \geq 0$ for all $i, j \in \{1, 2, \dots, N\}$) and suppose that $B = [b_{i,j}]$ is the matrix with entries $b_{i,j} = 1$ if $a_{i,j} > 0$ and $b_{i,j} = 0$ if $a_{i,j} = 0$. Assume that B is irreducible, then A has a positive eigenvalue λ with the following four properties:*

- (i) *There are positive vectors $\vec{\ell}$ and \vec{r} such that $\vec{\ell}A = \lambda\vec{\ell}$ and $A\vec{r} = \lambda\vec{r}$ called the left and right Frobenius–Perron eigenvectors respectively;*
- (ii) *The eigenvalue λ is simple;*
- (iii) *The spectrum of $\lambda^{-1}A$ consists of 1, several (potentially zero) roots of unity, and a finite subset of the open unit disc.*
- (iv) *If B is irreducible⁴ and aperiodic, then the spectrum of $\lambda^{-1}B$ consists of 1 and a finite subset of the open unit disc.*

The importance of this theorem will be realised throughout the remainder of this chapter.

The Frobenius–Perron Operator

Definition 2.2.2 (Frobenius–Perron Operator). Given a probability space $(\mathbb{X}, \mathcal{A}, \mu)$ and a non-singular transformation $T : \mathbb{X} \circlearrowright$, the *Frobenius–Perron operator* or *transfer operator*, $\mathcal{P} : L^1(\mathbb{X}) \circlearrowright$ is the unique⁵ operator that analyses an ensemble of trajectories (encoded as densities) of a dynamical system and is defined as

$$\int_A \mathcal{P}f(x) d\mu(x) = \int_{T^{-1}(A)} f(x) d\mu(x), \quad (2.2.1)$$

for all $f(x) \in L^1(\mathbb{X})$ and where $A \subseteq \mathbb{X}$. If A is given explicitly (e.g., an interval of the real line and $\mathbb{X} = \mathbb{R}$), then by differentiating both sides and applying the fundamental theorem of calculus, the transfer operator can be written explicitly in the form

$$\mathcal{P}f(x) = \frac{d}{dx} \int_{T^{-1}([a,x])} f(x') d\mu(x'), \quad a \in \mathbb{R}, \quad x \geq a. \quad (2.2.2)$$

Furthermore, if one assumes that $T(x)$ is invertible and differentiable, then by applying the chain rule and the fundamental theorem of calculus,

$$\mathcal{P}f(x) = \frac{d}{dx} \int_{T^{-1}(a)}^{T^{-1}(x)} f(x') d\mu(x') = f(T^{-1}(x)) \frac{d}{dx}(T^{-1}(x)) = \frac{f(T^{-1}(x))}{|T'(T^{-1}(x))|} \quad (2.2.3)$$

⁴Recall that a matrix B is *irreducible* if for every $1 \leq i, j \leq N$ there exists $n \geq 0$ such that $P_{i,j}^n > 0$. Figuratively speaking, P is irreducible if any outcome i can be followed by any outcome j , after a number of steps, which may or may not depend on i and j .

⁵Here, we refer to the uniqueness of the Lebesgue integral and not the operator itself. In fact, there are many other analytic settings for the Frobenius–Perron operator such as multi-dimensional, stochastic, and complex.

for all $x \in [a, b]$. It is however, possible that T is non-invertible, in which case the integral derivation is applied over the pre-images for the deterministic evolution of densities in maps,

$$\mathcal{P}f(x) = \sum_{y \in T^{-1}(x)} \frac{f(y)}{|T'(y)|}. \quad (2.2.4)$$

The Frobenius–Perron operator satisfies the following properties:

- (i) $\mathcal{P}(\alpha f + \beta g)(x) = \alpha \mathcal{P}f(x) + \beta \mathcal{P}g(x)$ for any $f(x), g(x) \in L^1(\mathbb{X})$ and constants $\alpha, \beta \in \mathbb{R}$ (linearity);
- (ii) $\mathcal{P}f(x) \geq 0$ if $f(x) \geq 0$ (positivity);
- (iii) $\int_{\mathbb{X}} \mathcal{P}f(x) d\mu(x) = \int_{\mathbb{X}} f(x) d\mu(x)$ for all $f(x) \in L^1(\mathbb{X})$ (integral-preserving); and
- (iv) $\|\mathcal{P}f(x)\|_1 \leq \|f(x)\|_1$ (non-expansive).

If an operator satisfies conditions 1, 2, and 4, it is called a *Markov operator*. We now illustrate an example of computing the action of the Frobenius–Perron operator on densities given a particular map.

Example 2.2.3. Consider the angle-doubling map, $T(x) : \mathbb{S}^1 \circlearrowright$ where $T(x) = 2x \bmod 1$ and the interval $I \subseteq \mathbb{S}$. Then the inverse of the period doubling map can be written as $T^{-1}(I) = I/2 \cup (1+I)/2$. Thus the transfer operator can then be computed using (2.2.4):

$$\begin{aligned} \int_I \mathcal{P}f(y) dy &= \int_{T^{-1}(I)} f(x) dx = \underbrace{\int_{I/2} f(x) dx}_{\text{substitute } x=y/2} + \underbrace{\int_{(1+I)/2} f(x) dx}_{\text{substitute } x=(y+1)/2} \\ &= \frac{1}{2} \left(\int_I f(y/2) dy + \int_I f((y+1)/2) dy \right) \\ &= \frac{1}{2} \int_I f(y/2) + f((y+1)/2) dy = \int_I \mathcal{P}f(y) dy. \end{aligned}$$

Given the current functional-analytic setup of the Frobenius–Perron operator, it is natural to consider the dual operator, which leads to the following:

The Koopman Operator

Definition 2.2.4 (Koopman Operator). Let $(\mathbb{X}, \mathcal{A}, \mu)$ be a probability space, $T : \mathbb{X} \circlearrowright$ a non-singular transformation, and a function $f(x) \in L^\infty(\mathbb{X})$. The operator $\mathcal{K} : L^\infty(\mathbb{X}) \circlearrowright$ given by

$$\mathcal{K}f(x) = f(T(x)), \quad (2.2.5)$$

is called the *Koopman operator* (or *composition operator*) with respect to T .

The Koopman operator was introduced by Koopman in 1931 and satisfies the following important properties:

- (i) $\mathcal{K}(\alpha f + \beta g)(x) = \alpha \mathcal{K}f(x) + \beta \mathcal{K}g(x)$ for all $f(x), g(x) \in L^\infty(\mathbb{X})$ and constants $\alpha, \beta \in \mathbb{R}$ (linearity);

- (ii) $\|\mathcal{K}f(x)\|_\infty \leq \|f(x)\|_\infty$ (non-expansive); and
- (iii) For any $f(x) \in L^1(\mathbb{X})$ and $g(x) \in L^\infty(\mathbb{X})$, $\langle \mathcal{P}f(x), g(x) \rangle = \langle f(x), \mathcal{K}g(x) \rangle$ (adjoint).

Unlike the Frobenius–Perron operator, the Koopman operator describes the action on *observables*, i.e., $\{f(T_n(x))\}_{n \in \mathbb{Z}}$ ($n \in \mathbb{Z}_+$ if non-invertible). The relationship between the two operators is via the adjoint property, i.e.,

$$\langle \mathcal{P}f(x), g(x) \rangle_\mu = \langle f(x), \mathcal{K}g(x) \rangle_\mu \quad (2.2.6)$$

where $\langle \cdot, \cdot \rangle_\mu$ denotes the duality pairing from $L^1(\mathbb{X})$ to $L^\infty(\mathbb{X})$ functions,

$$\langle f(x), g(x) \rangle_\mu = \int_{\mathbb{X}} f(x)g(x) d\mu(x).$$

Under certain conditions, the Koopman operator can also be defined on $L^2(\mathbb{X})$.

Spectral Properties of Transfer Operators

In this section, we consider the space of functions of *bounded variation*⁶ denoted by $\mathcal{V} = \mathcal{V}(I)$, a Banach space in which for a function $f(x) : I \rightarrow \mathbb{C}$, where $I = [a, b]$ is a compact interval of the real line, we have for each subinterval $J \subset I$:

$$\text{var}_J(f(x)) = \sup \left\{ \sum_{i=1}^n |f(x_i) - f(x_{i-1})| : n \geq 1, x_i \in J, x_0 < x_1 < \dots < x_n \right\}. \quad (2.2.7)$$

Moreover, we will denote by $\mathcal{N} = \mathcal{N}(I) \subset \mathcal{V}(I)$ the space of functions $f(x) \in \mathcal{V}(I)$ which vanish except on (at most) a countable set. Equation (2.2.7) is often referred to as the *total variation* and implies that if $\text{var}_J f(x) < \infty$ then $f(x)$ is bounded. Note that the total variation vanishes for constant functions, and is thus not a norm. However, one may endow \mathcal{V} with the norm

$$\|f(x)\|_{\mathcal{V}} = \text{var}_I(f(x)) + \sup_I \{|f(x)|\}.$$

We now recall some basic properties of \mathcal{V} :

- (i) \mathcal{V} is a Banach space for $\|\cdot\|_{\mathcal{V}}$;
- (ii) For all $x \neq b \in I$ and $z \neq a \in I$

$$\lim_{y \downarrow x} \text{var}_{(x,y]} f(x) = 0, \quad \lim_{y \uparrow z} \text{var}_{[y,z)} f(x) = 0,$$

which further implies that the following limits exist for each $x \in (a, b)$

$$f(x_+) = \lim_{y \downarrow x} f(y), \quad f(x_-) = \lim_{y \uparrow x} f(y)$$

and that $f(a_+)$ and $f(b_-)$ are well-defined⁷.

- (iii) The set of discontinuities $\{x : f(x_\pm) \neq f(x)\}$ of $f(x)$ is at most countable;

⁶We consider this space in order to preserve the measure of weighted transfer operators (i.e., the Frobenius–Perron operator).

⁷Assuming that $a < b$, we write $f(a_-) = f(a)$ and $f(b_+) = f(b)$.

(iv) For any $f(x), g(x) \in \mathcal{V}$, we have a “primitive version” of the Leibniz formula,

$$\text{var}(f(x)g(x)) \leq \sup |f(x)| \text{var } g(x) + \sup |g(x)| \text{var } f(x);$$

and

(v) If $f(x) \in \mathcal{V}$ is real-valued, then the two non-negative functions given by $f_+(x) = \max\{f(x), 0\}$ and $f_-(x) = -\min\{f(x), 0\}$ are of bounded variation.

Consider equation (2.2.4), this is actually a special case of a more general case of the transfer operator with a weighting function $w(x) = 1/|T'(x)|$ in which the following results hold. We will assume that $w(x)$ is non-negative and is *piecewise monotone* — that is:

Definition 2.2.5 (Piecewise monotone). Consider the compact interval $I = [a, b] \subset \mathbb{R}$. Then $T : I \circlearrowright$ is piecewise monotone if there exists $N \geq 1$ and a corresponding sequence $a = a_0 < a_1 < \dots < a_N = b$ such that $T|_{(a_i, a_{i+1})}$ is continuous and strictly monotone for all i .

We now define the spectral radii⁸ for the Frobenius–Perron operator and its dual as

$$R_{\mathcal{P}} = \lim_{n \rightarrow \infty} (\|\mathcal{P}^n\|_{\infty})^{1/n} = \lim_{n \rightarrow \infty} (\mathcal{P}^n 1)^{1/n}, \quad (2.2.8)$$

$$R_{\mathcal{K}} = \lim_{n \rightarrow \infty} (\|\mathcal{K}^n\|_{\infty})^{1/n} = \lim_{n \rightarrow \infty} \left(\left\| \frac{1}{|T'(x)|^n} \right\|_{\infty} \right)^{1/n}, \quad (2.2.9)$$

which implies that $R_{\mathcal{K}} \leq R_{\mathcal{P}}$. We now state the main theorem on the essential spectral radius of the transfer and composition operators, without proof. For a complete proof (and further details on the spectral properties of the transfer operators), see [2].

Theorem 2.2.6 (Essential spectral radius on \mathcal{V}/\mathcal{N}).

- (i) For a function $f(x) \in \mathcal{V}/\mathcal{N}$, we have that $R_{\mathcal{P}} \leq R_{\mathcal{K}}$;
- (ii) The spectral radius of $R(\mathcal{P})$ of the transfer operator on \mathcal{V}/\mathcal{N} satisfies $R(\mathcal{P}) \leq R_{\mathcal{P}}$; and
- (iii) If $w(x)$ is real and non-negative, then $R(\mathcal{P}) = R_{\mathcal{P}}$. Moreover, if $R_{\mathcal{K}} < R_{\mathcal{P}}$, then $R_{\mathcal{P}}$ is an eigenvalue with non-negative eigenfunction $f_w(x)$, and there exists an eigenfunctional ν_w of \mathcal{K} for R , with ν_w a Borel probability measure and $\nu_w f(x) > 0$. The measure ν_w is atomless.

Proposition 2.2.7 (Spectrum on \mathcal{V} or \mathcal{N}). The spectrum of the Frobenius–Perron operator⁹ $\mathcal{P}_w : \mathcal{V} \circlearrowright$ outside of the disc of radius

$$\tilde{R} = \lim_{n \rightarrow \infty} (\sup_I |w^n(x)|)^{1/n}$$

coincides with the spectrum of \mathcal{P}_w on \mathcal{N} outside of the disc \tilde{R} . Furthermore, it consists of isolated eigenvalues of finite multiplicity.

⁸Note that these are written in terms of the L^∞ norm while $R(\cdot)$ is in terms of the bounded variation norm.

⁹Remember that this is for the weighted transfer operator, which means it holds for the same transfer operator defined by equation (2.2.4).

Theorem 2.2.8. *The Frobenius–Perron operator $\mathcal{P} : \mathcal{V} \circlearrowleft$ is quasi-compact¹⁰ on \mathcal{V} with the norm $\|f\| = \max\{\|f\|_1, \text{var}(f)\}$. Furthermore, the essential spectral radius of \mathcal{P} , denoted by $\sigma_e(\mathcal{P})$ is contained inside a disc of radius $R_e = \sup\{|\lambda| : \lambda \in \sigma_e(\mathcal{P})\}$, where the spectral radius is defined by*

$$R = \lim_{k \rightarrow \infty} \left(\sup_x \frac{1}{|(T^k)'(x)|} \right)^{1/k}. \quad (2.2.10)$$

The spectral points of the Frobenius–Perron operator outside of the disc $\{z \in \mathbb{C} : |z| \leq R_e\}$ are isolated eigenvalues of \mathcal{P} (with finite multiplicity).

Although we shall not prove this result, it makes use of the following spectral inclusion (which will be useful to us in the following chapter):

$$\sigma(\mathcal{P}) \subset \sigma(\mathcal{P}|_{\mathcal{N}}) \cup \sigma(\mathcal{P}^{\mathcal{V}/\mathcal{N}}), \quad \sigma(\mathcal{P}^{\mathcal{V}/\mathcal{N}}) \subset \sigma(\mathcal{P}|_{\mathcal{N}}) \cup \sigma(\mathcal{P}) \quad (2.2.11)$$

where $\mathcal{P}^{\mathcal{V}/\mathcal{N}}$ denotes the the Frobenius–Perron operator induced by \mathcal{P} on \mathcal{V}/\mathcal{N} .

For a given Frobenius–Perron operator acting on a Banach space, $\mathcal{P} : (\mathbb{X}, \|\cdot\|) \circlearrowleft$, it is known that a perturbation \mathcal{P}_ε , of said operator, does not necessarily converge in norm, i.e.,

$$\lim_{\varepsilon \rightarrow 0} \|\mathcal{P}_\varepsilon - \mathcal{P}\| \neq 0. \quad (2.2.12)$$

However, if we can equip the Banach space with an additional norm, then one can introduce a *triple norm*, or *asymmetric operator norm*,

$$\|\mathcal{P}\| = \sup_{\|\varphi\| \leq 1} |\mathcal{P}\varphi|, \quad \mathcal{P} : (\mathbb{X}, \|\cdot\|) \rightarrow (\mathbb{Y}, |\cdot|), \quad (2.2.13)$$

where $(\mathbb{X}, \|\cdot\|)$ and $(\mathbb{Y}, |\cdot|)$ are Banach spaces satisfying $\mathbb{X} \subset \mathbb{Y}$ and $|\varphi| \leq \|\varphi\|$ for all $\varphi \in \mathbb{X}$, then we can show that (2.2.12) holds under certain conditions (and thus a triple norm is a weaker notion). This particular result is due to Keller and Liverani in [14]:

Theorem 2.2.9 (Keller–Liverani). *Let \mathcal{P}_ε with $\varepsilon > 0$ be a family of operators satisfying:*

(A1) For every $\varepsilon \geq 0$, the operator $\mathcal{P}_\varepsilon : \mathcal{B} \circlearrowleft$ is bounded for $|\cdot|$, with

$$\sup_{\varepsilon \geq 0} \sup_{n \in \mathbb{Z}_+} |\mathcal{P}_\varepsilon^n| < \infty.$$

(A2) There are constants $\kappa < 1$, $C > 0$ such that for all $n \in \mathbb{Z}_+$, there exists an $\varepsilon(n)$ so that for every $\varepsilon < \varepsilon(n)$ and all $\varphi \in \mathcal{B}$,

$$\|\mathcal{P}_\varepsilon^n \varphi\| \leq C(\kappa^n \|\varphi\| + |\varphi|).$$

(A3) For each $\varepsilon \geq 0$, the essential spectral radius of \mathcal{P}_ε on $(\mathcal{B}, \|\cdot\|)$ is bounded by κ .

(A4) There is a monotone upper semi-continuous function¹¹ τ on $[0, \infty)$, with $\tau(\varepsilon) > 0$ for $\varepsilon > 0$, and $\lim_{\varepsilon \rightarrow 0} \tau(\varepsilon) = 0$, so that for each small enough ε ,

$$\|\mathcal{P}_0 - \mathcal{P}_\varepsilon\| \leq \tau(\varepsilon).$$

¹⁰Quasi-compactness is a property that ensures the spectrum of the transfer operator can be broken up into an isolated part, and a non-isolated part, where the spectrum greater than the essential spectral radius has eigenvalues of finite multiplicity.

¹¹Recall that a function $f(x)$ is *upper semi-continuous* at x_0 if for every $\varepsilon > 0$, there exists a neighbourhood U of x_0 such that $f(x) \leq f(x_0) + \varepsilon$ for all $x \in U$ and $f(x) > -\infty$ (when $f(x_0) \neq -\infty$).

Then, under these assumptions, there exists $\delta > 0$ such that if $\varepsilon > 0$ is sufficiently small, for every $1 \leq j \leq l$, the spectral projections acting on the perturbed operator \mathcal{P}_ε ,

$$\Pi_j^{\varepsilon, \delta} \equiv \frac{1}{2\pi i} \oint_{\partial B_\delta(r_j)} (z - \mathcal{P}_\varepsilon)^{-1} dz$$

are well-defined for arbitrary but sufficiently small δ , and satisfy

$$\lim_{\varepsilon \rightarrow 0} \|\Pi_j^{\varepsilon, \delta} - \Pi_j^{0, \delta}\| = 0.$$

Furthermore, the ranks of $\Pi_j^{\varepsilon, \delta}$ and $\Pi_j^{0, \delta}$ coincide and for $|r| > \alpha$, letting

$$\Pi_r^\varepsilon \equiv \frac{1}{2\pi i} \oint_{\partial B_r(0)} (z - \mathcal{P}_\varepsilon)^{-1} dz,$$

then we have

$$\lim_{\varepsilon \rightarrow 0} \|\Pi_r^\varepsilon - \Pi_r^0\| = 0.$$

Finally, there exists $K = K(\delta, r) > 0$ such that for each $\varepsilon > 0$ sufficiently small and for all $n \in \mathbb{N}$,

$$\|\mathcal{P}_\varepsilon^n \Pi_r^\varepsilon\| \leq Kr^n.$$

The importance of this theorem is recognised through the fact that this result ensures the stability of the spectrum of the transfer operator under perturbations — which is crucial to the numerical methods employed in the following sections.

2.2.1 Semigroups for Transfer Operators

As we will see in chapter 3, the semigroup setting for continuous-time transfer operators is crucial for the numerical methods discussed in recent papers. In addition, all of the linear functional analysis techniques used in the discrete-time setting above remains available. The distinction between continuous-time and discrete-time settings are paramount to understanding how different phenomena arise in dynamical systems. For example, one crucial difference is the number of dimensions required for chaotic behaviour to arise in a system, which is three for continuous time, whereas one can observe chaotic behaviour in very simple one-dimensional maps such as the logistic map.

The Frobenius–Perron Operator

Definition 2.2.10 (Frobenius–Perron operator). Given a measure μ on \mathbb{X} and that all transformations T_t of a given semidynamical system $\{T_t\}_{t \geq 0}$ are non-singular. Then analogously to (2.2.1), we have

$$\int_A \mathcal{P}_t f(x) d\mu(x) = \int_{T_t^{-1}(A)} f(x) d\mu(x), \quad A \in \mathcal{A}, \tag{2.2.14}$$

for fixed $t \geq 0$, uniquely defines the *Frobenius–Perron operator* $\mathcal{P}_t : L^1(\mathbb{X}) \circlearrowleft$ corresponding to the semidynamical system $\{T_t\}_{t \geq 0}$.

Similarly to (2.2.1), the Frobenius–Perron operator for semigroups satisfies the following:

- (i) $\mathcal{P}_t(\alpha f + \beta g)(x) = \alpha \mathcal{P}_t f(x) + \beta \mathcal{P}_t g(x)$ for all $f(x), g(x) \in L^1(\mathbb{X})$ and constants $\alpha, \beta \in \mathbb{R}$ (linearity);
- (ii) $\mathcal{P}_t f(x) \geq 0$ implies $f(x) \geq 0$ (positivity); and
- (iii) $\int_{\mathbb{X}} \mathcal{P}_t f(x) d\mu(x) = \int_{\mathbb{X}} f(x) d\mu(x)$ for all $f(x) \in L^1(\mathbb{X})$ (integral-preserving).

As expected, for each fixed time $t \geq 0$, $\mathcal{P}_t : L^1(\mathbb{X}) \circlearrowright$ is also a Markov operator. If in addition to the conditions above, (2.2.14) satisfies

- (iv) $\mathcal{P}_{s+t} f(x) = \mathcal{P}_s(\mathcal{P}_t f)(x)$ for $f(x) \in L^1(\mathbb{X})$ and $s, t \in \mathbb{R}_+$; and
- (v) $\mathcal{P}_0 f(x) = f(x)$ for all $f(x) \in L^1(\mathbb{X})$;

then on a probability space $(\mathbb{X}, \mathcal{A}, \mu)$, we call the family of operators $\mathcal{P}_t : L^1(\mathbb{X}) \circlearrowright$ a *stochastic semigroup*, or *probability semigroup*. Furthermore, if for each $f(x) \in L^1(\mathbb{X})$ and $t_0 \geq 0$ we have

$$\lim_{t \rightarrow t_0} \|\mathcal{P}_t f(x) - \mathcal{P}_{t_0} f(x)\| = 0,$$

then the stochastic semigroup formed by \mathcal{P}_t is called *continuous*¹². Similar to the non-expansive property, a property shared by stochastic semigroups of the Frobenius–Perron operator is that

$$\|\mathcal{P}_t f(x) - \mathcal{P}_t g(x)\| \leq \|f(x) - g(x)\|$$

for any two functions $f(x), g(x) \in L^1(\mathbb{X})$. As a result, the function $t \mapsto \|\mathcal{P}_t f(x) - \mathcal{P}_t g(x)\|$ is non-increasing in t . One should note that although the theory of semigroups has been presented with motivation of transfer operators, it is not necessarily restricted to dynamical systems.

The Koopman Operator

Definition 2.2.11 (Koopman operator). Let $\{T_t\}_{t \geq 0}$ be a semigroup of non-singular transformations T_t [$\mu(A) = 0$ implies $\mu(T_t^{-1}(A) = 0)$] on the probability space $(\mathbb{X}, \mathcal{A}, \mu)$. Further, let $f(x) \in L^\infty(\mathbb{X})$, then associate $\mathcal{K} : L^\infty(\mathbb{X}) \circlearrowright$ given by

$$\mathcal{K}_t f(x) = f(T_t(x)), \quad (2.2.15)$$

as the *Koopman operator* of T_t .

As before, the Koopman operator for semigroups satisfies the following:

- (i) $\mathcal{K}(\alpha f + \beta g)(x) = \alpha \mathcal{K}f(x) + \beta \mathcal{K}g(x)$ for all $f(x), g(x) \in L^\infty(\mathbb{X})$ and constants $\alpha, \beta \in \mathbb{R}$ (linearity);
- (ii) For any $f(x) \in L^1(\mathbb{X})$ and $g(x) \in L^\infty(\mathbb{X})$, $\langle \mathcal{P}_t f(x), g(x) \rangle = \langle f(x), \mathcal{K}_t g(x) \rangle$ for any $t \geq 0$ (adjoint);
- (iii) $\mathcal{K}_{s+t} f(x) = \mathcal{K}_s(\mathcal{K}_t f)(x)$ for $f(x) \in L^\infty(\mathbb{X})$ and $s, t \in \mathbb{R}_+$ (semigroup); and
- (iv) $\mathcal{K}_0 f(x) = f(x)$ for each $f(x) \in L^\infty(\mathbb{X})$ (identity).

¹²Those familiar with stochastic processes may also call this *Feller*.

The family of Koopman operators $\{\mathcal{K}_t\}_{t \geq 0}$ is a semigroup but in general, is not a stochastic semigroup (since \mathcal{K}_t does not map $L^1(\mathbb{X})$ into itself). Instead of preserving the norm, the Koopman operator satisfies

$$\text{ess sup } |\mathcal{K}_t f(x)| \leq \text{ess sup } |f(x)|.$$

Although the Frobenius–Perron and Koopman operators do not share the stochastic semigroup property, we can still introduce a common notion for their respective families, $\{\mathcal{P}_t\}_{t \geq 0}$ and $\{\mathcal{K}_t\}_{t \geq 0}$ through the following definition.

Definition 2.2.12 (Semigroup of contractions). Let $1 \leq p \leq \infty$. Then a family of operators $\{T_t\}_{t \geq 0}$ with $T_t : L^p(\mathbb{X}) \rightarrow L^p(\mathbb{X})$ is called a *semigroup of contracting linear operators* or a *semigroup of contractions* if T_t satisfies the following:

- (i) $T_t(\alpha f + \beta g)(x) = \alpha T_t f(x) + \beta T_t g(x)$ for $f(x), g(x) \in L^p(\mathbb{X})$ and $\alpha, \beta \in \mathbb{R}$ (linearity);
- (ii) $\|T_t f(x)\|_p \leq \|f(x)\|_p$ for each $f(x) \in L^p(\mathbb{X})$ (non-expansive);
- (iii) $T_0 f(x) = f(x)$ for all $f(x) \in L^p(\mathbb{X})$ (identity); and
- (iv) $T_{s+t} f(x) = T_s(T_t f)(x)$, for any $f(x) \in L^p(\mathbb{X})$ (semigroup).

Similar to before, if the semigroup $\{T_t\}_{t \geq 0}$ satisfies

$$\lim_{t \rightarrow t_0} \|T_t f(x) - T_{t_0} f(x)\|_p = 0,$$

for $f(x) \in L^p(\mathbb{X})$ and $t_0 \geq 0$, then this semigroup is called *continuous*.

The common property shared by the Frobenius–Perron and Koopman operators for semigroups will allow us to investigate the functional-analytic relationships.

Infinitesimal Operators for Dynamical Systems

Arguably, the main difficulty that arises in continuous-time dynamical systems is the question of continuity with respect to time. Although it may appear more difficult to handle than discrete-time settings, we also have new tools to handle such detail — the infinitesimal generator.

Definition 2.2.13 (Infinitesimal generator). Let $1 \leq p \leq \infty$ and $\{T_t\}_{t \geq 0}$ be a semigroup of contractions. Then for all $f(x) \in L^p(\mathbb{X})$ that also satisfy the limit (in the strong sense of convergence)

$$\mathcal{G} f(x) = \lim_{t \downarrow 0} \frac{T_t f(x) - f(x)}{t}, \quad (2.2.16)$$

we say that $f(x)$ is in the linear subspace $D(\mathcal{G})$. Equation (2.2.16) is called the *infinitesimal operator* or *infinitesimal generator* and is a mapping, $\mathcal{G} : D(\mathcal{G}) \rightarrow L^p(\mathbb{X})$.

We now turn to deriving the infinitesimal operator for both the Frobenius–Perron and Koopman operators that are generated by d -dimensional autonomous systems of ordinary differential equations,

$$\frac{dx}{dt} = F(x),$$

where $x = (x_1, \dots, x_d)$ and $F(x) = (F_1(x), \dots, F_d(x))$. First, we derive the infinitesimal generator, \mathcal{G}_K , for the Koopman operator and then exploit duality to get the Frobenius–Perron generator. The semigroup of transformations that corresponds to this system is defined by

$$T_t(x(0)) = x(t), \quad (2.2.17)$$

where $x(t)$ is the solution with initial condition $x(0)$. Assuming that the vector field $F(x) = (F_1(x), \dots, F_d(x))$ has continuous partial derivatives in all variables and that for all initial conditions, the solution $x(t)$ exists for all $t \in \mathbb{R}$, we proceed as follows for the generator of the Koopman operator. By definition,

$$\mathcal{K}_t f(x(0)) = f(T_t(x(0)))$$

and therefore

$$\frac{\mathcal{K}_t f(x(0)) - f(x(0))}{t} = \frac{f(T_t(x(0))) - f(x(0))}{t} = \frac{f(x(t)) - f(x(0))}{t}.$$

This implies that if f is continuously differentiable and has compact support, then by the mean value theorem, we have for some $0 < \theta < 1$,

$$\frac{\mathcal{K}_t f(x(0)) - f(x(0))}{t} = \sum_{i=1}^d f_{x_i}(x(\theta t)) x'_i(\theta t) = \sum_{i=1}^d f_{x_i}(x(\theta t)) F_i(x(\theta t)).$$

Using the semigroup of transformations, (2.2.17), we obtain

$$\frac{\mathcal{K}_t f(x(0)) - f(x(0))}{t} = \sum_{i=1}^d f_{x_i}(T_{\theta t}(x(0))) F_i(T_{\theta t}(x(0))), \quad (2.2.18)$$

and since the derivatives f_{x_i} are continuous and have compact support, we have for all $i = 1, \dots, d$,

$$\lim_{t \downarrow 0} f_{x_i}(T_{\theta t}(x(0))) F_i(T_{\theta t}(x(0))) = f_{x_i}(x(0)) F_i(x(0))$$

uniformly¹³ for all initial conditions $x(0)$. Thus (2.2.18) has a strong limit in $L^\infty(\mathbb{X})$, and therefore conclude that the infinitesimal operator \mathcal{G}_K is given by

$$\mathcal{G}_K f(x) = \sum_{i=1}^d \frac{\partial f(x)}{\partial x_i} F_i(x). \quad (2.2.19)$$

We shall derive the infinitesimal generator for the Frobenius–Perron operator, but to do as done before with the Koopman operator would not be a trivial task. Instead, we recall that these two operators are adjoint — that is,

$$\langle \mathcal{P}_t f(x), g(x) \rangle = \langle f(x), \mathcal{K}_t g(x) \rangle \quad (2.2.20)$$

for $f(x) \in L^1(\mathbb{X})$ and $g(x) \in L^\infty(\mathbb{X})$. Now subtracting $\langle f(x), g(x) \rangle$ and dividing by t on both sides of equation (2.2.20), we have that

$$\langle (\mathcal{P}_t f(x) - f(x))/t, g(x) \rangle = \langle f(x), (\mathcal{K}_t g(x) - g(x))/t \rangle. \quad (2.2.21)$$

¹³Recall that a function $f : \mathbb{X} \rightarrow \mathbb{Y}$ is *uniformly continuous* if for two metric spaces (\mathbb{X}, d_1) , (\mathbb{Y}, d_2) and for every real number $\varepsilon > 0$, there exists a constant $\delta > 0$ such that for any $x, y \in \mathbb{X}$, if $d_1(x, y) < \delta$, then $d_2(f(x), f(y)) < \varepsilon$.

Now we let $f(x) \in D(\mathcal{G}_\mathcal{P})$ and $g(x) \in D(\mathcal{G}_\mathcal{K})$, where $\mathcal{G}_\mathcal{P}$ and $\mathcal{G}_\mathcal{K}$ denote the infinitesimal generators for the Frobenius–Perron and Koopman operators respectively. Taking the limit as $t \downarrow 0$ in (2.2.21) we obtain

$$\langle \mathcal{G}_\mathcal{P} f(x), g(x) \rangle = \langle f(x), \mathcal{G}_\mathcal{K} g(x) \rangle \quad (2.2.22)$$

and using the explicit form for the Koopman generator, i.e., (2.2.19), we see that if we write out the inner product explicitly and noting that $\mathbb{X} = \mathbb{R}^d$ and $d\mu = dx_1 \cdots dx_d = dx$, we have

$$\begin{aligned} \left\langle f(x), \sum_{i=1}^d F_i(x) \frac{\partial g}{\partial x_i} \right\rangle &= \int_{\mathbb{R}^d} f(x) \sum_{i=1}^d F_i(x) \frac{\partial g}{\partial x_i} dx \\ &= \sum_{i=1}^d \int_{\mathbb{R}^d} \left(\frac{\partial(fF_i g)}{\partial x_i} - g(x) \frac{\partial(fF_i)}{\partial x_i} \right) dx \end{aligned}$$

assuming both $f(x)$ and $g(x)$ are continuously differentiable. Since $g(x)$ has compact support, then

$$\sum_{i=1}^d \int_{\mathbb{R}^d} \frac{\partial(fF_i g)}{\partial x_i} dx = 0$$

and therefore

$$\left\langle f(x), \sum_{i=1}^d F_i(x) \frac{\partial g}{\partial x_i} \right\rangle = - \sum_{i=1}^d \int_{\mathbb{R}^d} g(x) \frac{\partial(fF_i)}{\partial x_i} dx = \left\langle - \sum_{i=1}^d \frac{\partial(fF_i)}{\partial x_i}, g(x) \right\rangle.$$

Using this formula and the adjoint relation (2.2.22) we obtain that

$$\langle \mathcal{G}_\mathcal{P} f(x), g(x) \rangle = \left\langle - \sum_{i=1}^d \frac{\partial(fF_i)}{\partial x_i}, g(x) \right\rangle$$

which holds for continuously differentiable functions $f(x) \in D(\mathcal{G}_\mathcal{P})$ and continuously differentiable functions $g(x)$ with compact support. Hence the infinitesimal generator for the Frobenius–Perron operator is given by

$$\mathcal{G}_\mathcal{P} f(x) = - \sum_{i=1}^d \frac{\partial(fF_i)}{\partial x_i}. \quad (2.2.23)$$

One may also show that for a function $u(t, x) = \mathcal{K}_t f(x)$ (resp. $u(t, x) = \mathcal{P}_t f(x)$) that satisfies certain properties, then these relationships satisfy (respectively) the following partial differential equations (continuity equations)

$$\frac{\partial u}{\partial t} = + \sum_{i=1}^d \frac{\partial(uF_i)}{\partial x_i} \quad \text{and} \quad \frac{\partial u}{\partial t} = - \sum_{i=1}^d \frac{\partial(uF_i)}{\partial x_i}.$$

2.2.2 Establishing the Relationship Between the Frobenius–Perron and Koopman Operators

It was already identified that for $f(x) \in L^1(\mathbb{X})$ and $g(x) \in L^\infty(\mathbb{X})$, that the Frobenius–Perron and Koopman operators are adjoint to each other. However, it is possible to

establish these operators (respectively) as a “push-forward” on a density and a “pull-back” on a function. More precisely, consider the semigroups of the Frobenius–Perron and Koopman operators, $\{\mathcal{P}_t\}$ and $\{\mathcal{K}_t\}$, generated by the same semi-dynamical system $\{T_t\}_{t \geq 0}$. Using the adjoint property, we may write explicitly,

$$\int_{\mathbb{X}} g(x) \mathcal{P}_t f(x) d\mu(x) = \int_{\mathbb{X}} f(x) g(T_t(x)) d\mu(x)$$

with $f(x) \in L^1(\mathbb{X})$ and $g(x) \in L^\infty(\mathbb{X})$. For some arbitrary subset $A \subset \mathbb{X}$ such that $A, T_t(A) \in \mathcal{A}$, define

$$f(x) = \mathbb{1}_A(x) \quad \text{and} \quad g(x) = \mathbb{1}_{\mathbb{X} \setminus T_t(A)}.$$

Substituting these into the preceding equation, we see that it becomes

$$\begin{aligned} \int_{\mathbb{X}} \mathbb{1}_{\mathbb{X} \setminus T_t(A)} \mathcal{P}_t f(x) d\mu(x) &= \int_{\mathbb{X}} f(x) \mathbb{1}_{\mathbb{X} \setminus T_t(A)}(T_t(x)) d\mu(x) \\ &= \int_A f(x) \mathbb{1}_{\mathbb{X} \setminus T_t(A)}(T_t(x)) d\mu(x). \end{aligned}$$

Since $T_t(A) \notin \mathbb{X} \setminus T_t(A)$, the right-hand side of this equation is zero. On the other hand, the left-hand side is just the $L^1(\mathbb{X})$ norm of the integrand, which implies that

$$\|\mathbb{1}_{\mathbb{X} \setminus T_t(A)} \mathcal{P}_t f(x)\|_1 = 0$$

and therefore

$$\mathcal{P}_t f(x) = 0$$

for $x \notin T_t(A)$. Hence the Frobenius–Perron operator can be viewed as a “push-forward”, sending a function supported on A in time to a function supported on a subset of $T_t(A)$. In a similar manner, consider the definition of the Koopman operator,

$$\mathcal{K}_t f(x) = f(T_t(x)).$$

Assuming that $f(x) \in L^\infty(\mathbb{X})$ is compact on a set A , e.g., $f(x) = \mathbb{1}_A(x)$, then we have

$$f(T_t(x)) = 0$$

if $T_t(x) \notin A$, which in turn, implies that

$$\mathcal{K}_t f(x) = 0 \tag{2.2.24}$$

for $x \notin T_t^{-1}(A)$. Figuratively speaking, one may view the Koopman operator as a “pull-back” on a function, sending the support from the set A backward in time to $T_t^{-1}(A)$. Furthermore, if we allow the semi-dynamical system to become a dynamical system, $\{T_t\}_{t \in \mathbb{R}}$ with T_t non-singular, then $T_t^{-1}(x) = T_{-t}(x)$ and thus (2.2.24) becomes

$$\mathcal{K}_t f(x) = 0$$

for $x \notin T_{-t}(A)$. If we further assume that the group $\{T_t\}_{t \in \mathbb{R}}$ preserves the measure μ , then we have

$$\int_A \mathcal{P}_t f(x) d\mu(x) = \int_{T_{-t}(A)} f(x) d\mu(x) = \int_A f(T_{-t}(x)) d\mu(x),$$

which means $\mathcal{P}_t f(x) = f(T_{-t}(x))$, or more importantly,

$$\mathcal{P}_t f(x) = \mathcal{K}_{-t} f(x). \quad (2.2.25)$$

This makes the comment regarding the continuity equations more explicit. In fact, for $f(x)$ in a dense subset of $L^1(\mathbb{X})$, we see that by applying the infinitesimal generator to (2.2.25), then

$$\mathcal{G}_{\mathcal{P}} f(x) = -\mathcal{G}_{\mathcal{K}} f(x).$$

In terms of Hilbert spaces, (i.e., $L^2(\mathbb{X})$), this result simply means that the adjoint of \mathcal{P}_t is also its inverse, and hence $\{\mathcal{P}_t\}$ is a unitary operator.

A central topic of interest in functional analysis and a crucial object in the study of ergodic theory, is the existence and uniqueness of fixed points for certain operators. In a dynamical system, the invariant density represents some form of ‘equilibrium’, or ‘steady-state’ behaviour, which has applications outside of mathematics such as science and engineering. In probability theory, and in particular, the study of Markov chains, one may be interested in knowing the stationary distribution, which allows one to predict long-term behaviour of the process (assuming it exists). This motivates the following definition:

Definition 2.2.14 (Invariant Density). Let $(\mathbb{X}, \mathcal{A}, \mu)$ be a probability space and $T : \mathbb{X} \rightarrow \mathbb{X}$ a non-singular transformation, then an *invariant density* is a density¹⁴ function $f(x)$, that satisfies

$$\mathcal{P}f(x) = f(x). \quad (2.2.26)$$

In 1947, Ulam and von Neumann were able to determine that for a particular logistic map, $T(x) = 4x(1-x)$, the invariant density of the Frobenius–Perron operator is given by

$$f(x) = \frac{1}{\pi \sqrt{x(1-x)}},$$

where the $1/\pi$ factor ensures $f(x)$ is a density (in the probabilistic sense). To verify such a claim is not difficult, but few theoretical tools exist for determining the invariant density, in general. Furthermore, the Frobenius–Perron and Koopman operators are defined on infinite dimensional function spaces. So one may use numerical techniques in order to identify invariant densities and similar objects.

2.3 Ulam's Method

2.3.1 History and Theory

In 1960, S. Ulam conjectured [25] (among many other ideas) that:

- (i) A finite rank approximation of the transfer operator can be made via a Markov chain with transition matrix

$$\widehat{P}_{i,j} = \frac{\mu(\mathbb{B}_i \cap T^{-1}(\mathbb{B}_j))}{\mu(\mathbb{B}_i)}$$

where each of the boxes \mathbb{B}_i form a partition of the space, i.e., $\mathbb{B}_i \cap \mathbb{B}_j = \emptyset$ for $i \neq j$ and $\cup_i \mathbb{B}_i = \mathbb{X}$; and

¹⁴We mean this in the probabilistic sense, i.e., $f(x)$ is non-negative and integrates to 1.

2.3. ULAM'S METHOD

- (ii) The dominant eigenvector (with eigenvalue $\lambda_1 = 1$) weakly approximates the invariant density of the Frobenius–Perron operator¹⁵.

In this section, the goal will be to derive and describe Ulam's method and establish its importance to the measurable dynamics community.

Remark 2.3.1 (On the history of the convergence of Ulam's method). An essential question regarding any numerical scheme is, under what circumstances does the algorithm converge to the ideal case? In the case of Ulam's method, it is not quite clear what conditions are required for the transformation T in general settings. The first result of convergence was shown by Li [17] in 1976 under the condition that T was an expanding, piecewise continuous interval map. Ding and Zhou were able to generalise the result to higher dimensions [9] and Murray gave the rate of convergence [20]. More recent results have generalised Ulam's method to converge under stochastic perturbations and more general function spaces such as the fractional Sobolev spaces addressed in [11].

Ulam's method is an approach to approximating the action of the Frobenius–Perron operator based on the Galerkin method. The Galerkin method projects the infinite dimensional linear space $L^1(\mathbb{X})$ with basis functions $\{\varphi_i(x)\}_{i=1}^\infty$ onto the finite dimensional subspace Δ_N such that $\Delta_N = \text{span}\{\varphi_i(x)\}_{i=1}^N$. So the projection operator $\Pi_N : L^1(\mathbb{X}) \rightarrow \Delta_N(\mathbb{X})$ maps the infinite dimensional operator into a finite rank matrix. This can be expressed via the integral inner product,

$$P_{i,j} = \langle \mathcal{P}(\varphi_i(x)), \varphi_j(x) \rangle = \int_{\mathbb{X}} \mathcal{P}(\varphi_i(x)) \varphi_j(x) d\mu(x).$$

Hence it can be shown that using this projection, one can approximate the Frobenius–Perron operator from an infinite dimensional operator into a stochastic matrix in a finite-dimensional vector space. This process is outlined below.

Start by letting the collection $\{\mathbb{B}_i\}_{i=1}^N$ denote the partition of the system $(\mathbb{X}, \mathcal{A}, \mu, T)$ into disjoint boxes such that $\cup_i \mathbb{B}_i = \mathbb{X}$ and denote $\mathbb{1}_{\mathbb{B}_i}$ the indicator function on the i -th box. This restricts the action of the Frobenius–Perron operator to the basis of characteristic functions, $\{\mathbb{B}_1, \dots, \mathbb{B}_N\}$. Applying the projection operator from above to the indicator function over a box \mathbb{B}_i and \mathbb{B}_j , the matrix P has entries in i, j as

$$\begin{aligned} P_{i,j} &= \int_{\mathbb{X}} \mathcal{P}(\mathbb{1}_{\mathbb{B}_i}) \mathbb{1}_{\mathbb{B}_j} d\mu(x) = \int_{\mathbb{B}_j} \mathcal{P}(\mathbb{1}_{\mathbb{B}_i}) d\mu(x) \\ &= \int_{T^{-1}(\mathbb{B}_j)} \mathbb{1}_{\mathbb{B}_i} d\mu(x) = \mu(\mathbb{B}_i \cap T^{-1}(\mathbb{B}_j)) \end{aligned}$$

where μ denotes the Lebesgue measure. It is customary to normalise this result in order to make P a stochastic matrix, i.e.,

$$\widehat{P}_{i,j} = \frac{\mu(\mathbb{B}_i \cap T^{-1}(\mathbb{B}_j))}{\mu(\mathbb{B}_i)}. \quad (2.3.1)$$

Each of the entries, $\widehat{P}_{i,j}$ can then be interpreted as the ratio of the fraction of box \mathbb{B}_i that will be mapped inside the box \mathbb{B}_j after one iteration of the map T to the measure

¹⁵Recall that for all $\{f_n\}_{n=1}^\infty \in L^p(\mathbb{X})$ then f_n converges *weakly* to f^* , denoted by $f_n \xrightarrow{w} f^*$, if $\lim_{n \rightarrow \infty} \int_{\mathbb{X}} |f^*(x) - f_n(x)| h(x) dx = 0$ for all test functions, $h(x) \in L^q(\mathbb{X})$ where p and q are dual indices, i.e., $1/p + 1/q = 1$.

of $\mathbb{1}_{\mathbb{B}_j}$. Alternatively, one can use the probabilistic interpretation, that is, $\widehat{P}_{i,j}$ represents the action on discrete probability measures. So if $\vec{v} \geq 0$ is a probability vector (i.e., $\sum_i v_i = 1$) then the probability vector \vec{v}' given by $\vec{v}' = \vec{v}\widehat{P}$ is the push-forward of the probability vector \vec{v} under the discretised action of T . Hence distributions can be pushed forward by matrix multiplication. For those familiar with elementary probability, this is exactly analogous to a transition, or P matrix of a Markov chain. To compute an entry of the transition matrix, $\widehat{P}_{i,j}$, the standard approach is Monte-Carlo quadrature, i.e.,

$$\widehat{P}_{i,j} \approx \frac{1}{N} \sum_{n=1}^N \mathbb{1}_{\mathbb{B}_i}(T(x_n)), \quad (2.3.2)$$

where each of the points x_n are chosen i.i.d from each of the boxes \mathbb{B}_i according to a uniform distribution.

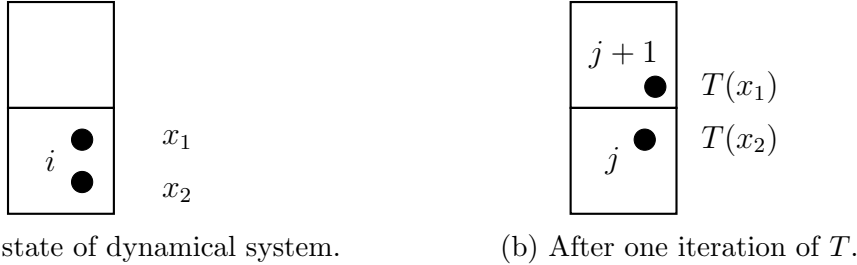


Figure 2.1: Visual representation of Ulam's method. Note that it is important to sample the same number of points from each box in order to capture all features of the dynamical system at a given resolution.

Now recall that a set E is called *invariant* if $\mu(T^{-1}(E)) = \mu(E)$ for some discrete-time map or $\mu(T_t^{-1}(E)) = \mu(E)$ for a continuous-time flow acting on a dynamical system. But consider a small perturbation on T , and denote it by \widetilde{T} . One would expect that for some metric ϱ that $\varrho(T(x), \widetilde{T}(x)) < \varepsilon$ for all $x \in \mathbb{X}$ and constant $\varepsilon > 0$. As a result, it can no longer be expected that all orbits will remain in the set $E \subset \mathbb{X}$, but measuring how far away from invariance a perturbed system is leads us to the following definition:

Definition 2.3.2 (Almost-invariant/Metastable). Given a set $E \subset \mathbb{X}$ and a transformation T_t on a probability space $(\mathbb{X}, \mathcal{A}, \mu)$, we call the set E *almost-invariant* or *metastable* with respect to a (not necessarily invariant) probability measure μ if

$$\varrho_\mu^t(E) = \frac{\mu(E \cap T_{-t}(E))}{\mu(E)} \approx 1,$$

for modest times t and where μ is typically taken to be the Lebesgue measure.

The purpose of introducing the concept of almost-invariant sets is to explain dynamical systems with a “leakage” type property such as a container filled with a liquid that has a hole, or a box full of particles with a small puncture in it. These are important as many real-world systems exhibit this property. For a more detailed exposition of the Ulam–Galerkin method, see [4]. A summary of the Ulam method is given in an algorithm below.

2.3. ULAM'S METHOD

Algorithm 1: Ulam's method

Input : Number of boxes N , flow (resp. map) T and time step t (resp. n), constant K for sampling per box.

Output: Ulam matrix P .

```

1 for  $i = 1 : N$  do
2   Sample  $K$  points from  $i$ th box  $\mathbb{B}_i$ 
3   Apply flow/map  $T$  for fixed time step ( $t$  or  $n$ )
4   for each box at time step  $t$ ,  $\mathbb{B}_i$  do
5     Apply equation (2.3.1) by counting the number of points in  $\mathbb{B}_i \cap T^{-1}(\mathbb{B}_j)$ 
      and normalise by dividing by  $\mu(\mathbb{B}_i)$ .
6   end
7 end
8 Compute the (left) eigenvector(s) by finding the right eigenvector(s) of the transpose of the matrix  $\widehat{P}$ .

```

Example 2.3.3 (Double-gyre). We consider the well-known non-autonomous system of differential equations called the *periodically driven double-gyre* and modify it so that it reads

$$\begin{aligned}\dot{x} &= -\pi A x \sin(\pi f(x, t)) \cos(\pi y) \\ \dot{y} &= +\pi A \cos(\pi f(x, t)) \sin(\pi y) f'(x, t)\end{aligned}$$

where $f'(x, t)$ is the derivative of $f(x, t)$ with respect to x and

$$f(x, t) = \delta \sin(\omega t)x^2 + (1 - 2\delta \sin(\omega t))x.$$

Here, δ is an arbitrary constant, the frequency $\omega > 0$ and A is the amplitude. For this example, $A = \delta = 1/4$ and $\omega = 2\pi$ (for unity period). A vector field plot can be seen below at time $t = 0$.

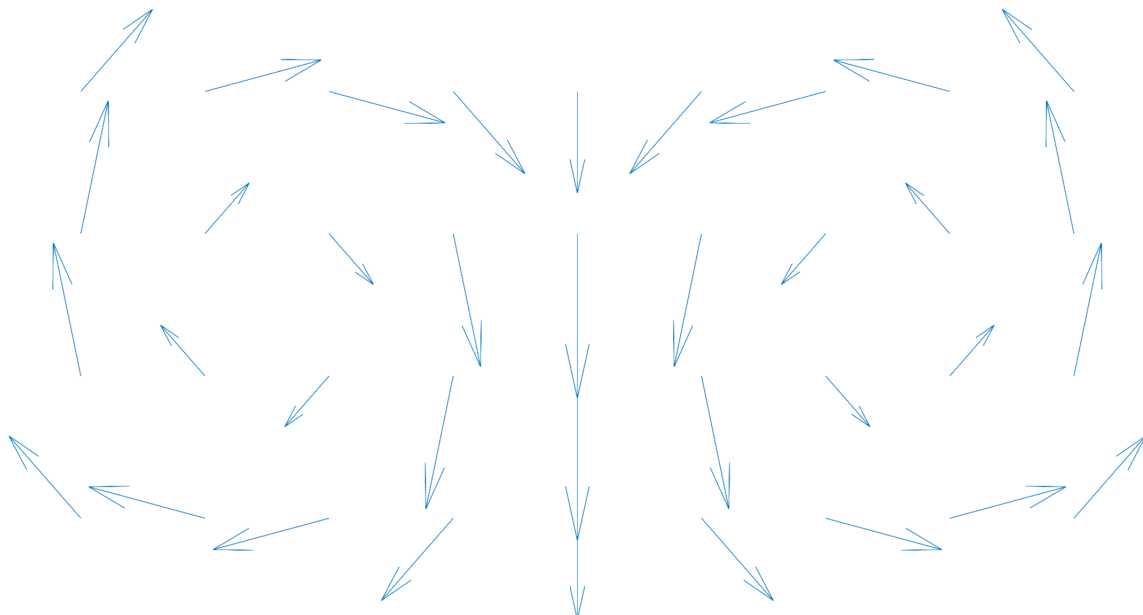
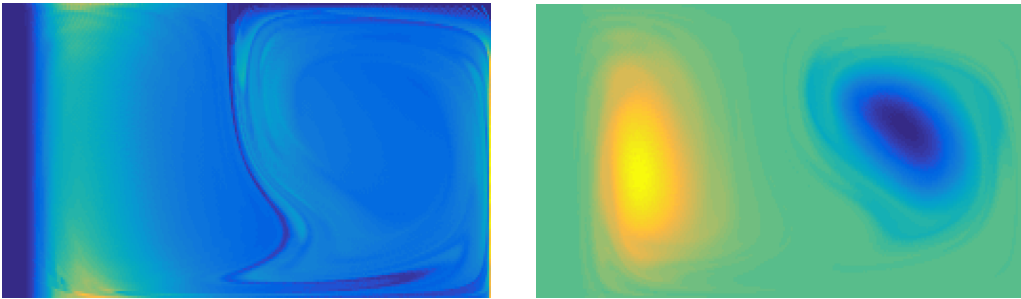


Figure 2.2: The original double-gyre system at the initial time $t = 0$.

By inspection, one would expect that there are two almost-invariant sets, and this is reflected in the eigenvectors below. See Figure 2.3 for the results of the MATLAB code

in Appendix A.1. In subsequent sections, we will make use of the isolated spectrum to detect eddies in systems more complicated than the double-gyre.



(a) The first left eigenvector of \hat{P} corresponds to the invariant density.
 (b) The second left eigenvector of \hat{P} describes the geometric convergence of the system.

Figure 2.3: Approximation to the eigenfunctions of the transfer operator for the double-gyre.

The geometric convergence will not be discussed here, however for the interested readers, we refer them to pages 85–89 of [4].

Remark 2.3.4. One may ask whether Ulam's method has more to offer if one were to use different basis functions, i.e., to use something other than the indicator function on boxes. Indeed, research has been conducted into the use of other basis functions such as higher order polynomials and trigonometric functions. One particular paper by Junge and Koltai [13] establish better algorithmic complexity than the traditional Ulam method described above. They achieve this by employing the *Haar wavelet*¹⁶, given by

$$\begin{aligned}\psi(x) &= \mathbb{1}_{x \in [0,1/2)} - \mathbb{1}_{x \in [1/2,1]} \\ \psi_{j,k}(x) &= \psi(2^j x - k),\end{aligned}$$

for all $j, k \in \mathbb{Z}$. In order to generalise this beyond the one-dimensional case, they use a tensor product construction and show that for functions with bounded first derivatives, then the algorithm converges with approximation error of $\mathcal{O}((N/2)^{d-1}2^{-N})$ and computational effort $\mathcal{O}((N/2)^{d-1}2^N)$ where N denotes the discretisation level (size of the matrix), 2^{-M} is the edge length of the boxes (in each direction), and d is the dimension of the phase space. Here, we have included the table detailing the asymptotic expressions for the cost and error of the Haar basis, and the standard basis. The authors concluded that after a certain threshold of desired accuracy, the sparse basis would become more efficient than the standard one.

	Cost	Error
Haar basis	$(N/2)^{d-1}2^N$	$(N/2)^{d-1}2^{-N}$
Standard basis	2^{dM}	2^{-M}

Table 2.4: A comparison of the computational complexity of the Haar basis and the standard basis for Ulam's method.

The authors also note that these improvements become more significant as the size of the data and dimension increases.

¹⁶The Haar wavelet was originally the subject of Alfred Haar's PhD thesis, in which he showed that the Haar functions form an orthonormal basis for $L^2[0, 1]$.

2.3.2 The Markov Partition and Other Considerations

Although Ulam's method can be applied to a wide variety of systems to approximate the invariant density, there are some special cases where we can exactly encode the action of the Frobenius–Perron and Koopman operators. This requires the introduction of a Markov partition:

Definition 2.3.5 (Markov partition). Let $T(x) : \mathbb{X} \rightarrow \mathbb{X}$ be a piecewise linear map on a metric space. A partition (modulo zero Lebesgue measurable sets) of \mathbb{X} into sets I_k is called *Markov*, or more commonly, a *Markov partition*, if for every natural numbers j, k in which $T(I_j)$ intersects the interior of I_k we have that $I_k \subset \overline{T(I_j)}$.

Figuratively speaking, this definition means that whenever an image rectangle intersects a partition element, the image must stretch across the entire expanding direction and be contained within the entire partition element in the contracting direction. More importantly, this implies that the dynamics of $T(x)$ can be encoded in an $n \times n$ transition matrix:

$$A_{j,k} = \begin{cases} 1 & \text{if } I_k \subset \overline{T(I_j)} \\ 0 & \text{otherwise.} \end{cases}$$

This implies that when a dynamical system has a Markov partition, Ulam's method yields an exact representation of the Frobenius–Perron operator. Now equipped with a numerical method for approximating invariant densities, we provide some numerical considerations.

Grid Refinement

Recall that the main object of interest when approximating the action of the Frobenius–Perron operator on a box \mathbb{B}_i is to estimate how much of \mathbb{B}_i maps across another box \mathbb{B}_j . From Ulam's conjecture,

$$P_{i,j} = \frac{\mu(\mathbb{B}_i \cap T^{-1}(\mathbb{B}_j))}{\mu(\mathbb{B}_i)} = \frac{1}{\text{area}(\mathbb{B}_i)} \int_{\mathbb{B}_i} \mathbb{1}_{T^{-1}(\mathbb{B}_j)}(x) d\mu(x)$$

where one recognises that this is in fact the spatial average. So the standard assumption for Monte Carlo integration applies here, i.e., drawing from the uniform distribution,

$$x \sim U(\mathbb{B}_i).$$

We shall note that by refining the grid we achieve two properties:

1. Improvements on Ulam's method and convergence. Much research has been dedicated to refinement, adaptive refinement, and rates of convergence.
2. Monte Carlo estimates of these integrals improve (assuming a finite-sized grid).

It has been shown that subdividing, or splitting regions equally with equal samples never increases the variance (even for Delaunay triangulation schemes¹⁷).

¹⁷This is a triangulation scheme that is popular in the finite element analysis literature, as well as computational geometry and computer science.

Continuity and Computational Complexity

Here, we discuss the relationship between Lipschitz continuity and computational effort of Ulam's method. We just discussed that unless a Markov partition is used, refining the grid in a compact space \mathbb{X} improves Monte Carlo approximations to the action of the Frobenius–Perron operator. For this discussion assume that the dynamical system is continuous in time and that the space \mathbb{X} has been partitioned into boxes \mathbb{B}_i (although the same results follow for triangulated tessellations, a box will make the arguments slightly easier) of length q . We will provide some considerations for how many points/samples are required in order to capture all the detail of the dynamics.

Let \mathbb{X} be compact and $f(t, x) : [t_0, t] \times \mathbb{X} \rightarrow \mathbb{X}$ be a flow. Consider a constant ε such that for every pair of solutions $x_1, x_2 \in \mathbb{X}$, in which at the initial time t_0 , $|x_1(t_0) - x_2(t_0)| < \varepsilon$ and $|x_1(t) - x_2(t)| < q$. More colloquially, this step asks that the distance between two initial conditions does not change too drastically. So we must control ε in order to ensure the final distance d between two points satisfies $d < q$. Recall that Gronwall's inequality states the following:

$$|x_1(t) - x_2(t)| \leq |x_1(t_0) - x_2(t_0)| e^{M|t-t_0|}$$

where M is the Lipschitz constant of $f(t, x)$. Assuming f is uniformly continuously differentiable, we have by the extreme value theorem,

$$M = \max_{(t,x) \in [t_0,t] \times \mathbb{X}} \left| \frac{\partial}{\partial x} f(t, x) \right|.$$

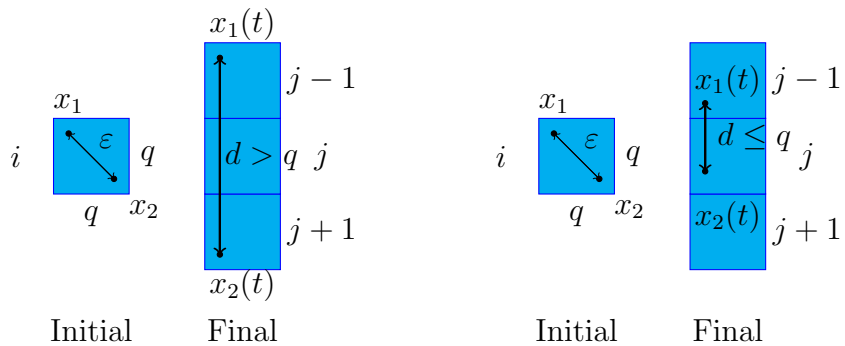
Hence we need to control the distance between $x_1(t)$ and $x_2(t)$ by controlling the distance between $x_1(t_0)$ and $x_2(t_0)$. Let

$$\varepsilon = \frac{q}{e^{M|t-t_0|}},$$

where we recall that q was the upper bound on the distance between two solutions at time t that started at a distance less than ε away at the initial time. Then using Gronwall's inequality and our initial hypothesis, we have

$$|x_1(t) - x_2(t)| \leq |x_1(t_0) - x_2(t_0)| e^{M|t-t_0|} < \varepsilon e^{M|t-t_0|} = q$$

for all $x(t) \in \mathbb{X}$ that satisfies $|x_1(t_0) - x_2(t_0)| < \varepsilon$.



- (a) Failure of sampling since the distance between the neighbouring points $x_1(t)$ and $x_2(t)$ is greater than the distance q of a single box element.
- (b) Here, the initial distance ε is small enough to ensure that the final distance between $x_1(t)$ and $x_2(t)$ is less than the element size q .

Figure 2.5: Demonstration of the Lipschitz continuity.

2.4 Literature Review

We now discuss the results and insights from more recent papers, making use of all the techniques previously discussed. These methods make extensive use of the spectral theoretic results previously established.

2.4.1 The Dellnitz–Froyland Ansatz

The “Dellnitz–Froyland” ansatz is attributed to the results on the isolated spectrum of the Frobenius–Perron operator as found in [7]. In particular, the authors discuss the existence of “large” isolated (non-unit by the Frobenius–Perron theorem) eigenvalues of the Frobenius–Perron operator. Here, large refers to the isolated eigenvalues greater than the *essential spectral radius*¹⁸ σ_e of a linear operator, the smallest non-negative number such that any eigenvalue in the spectrum outside the disk $\{z \in \mathbb{C} : |z| \leq \sigma_e\}$ is an isolated eigenvalue of finite (algebraic or geometric) multiplicity¹⁹ (see Figure 2.6).

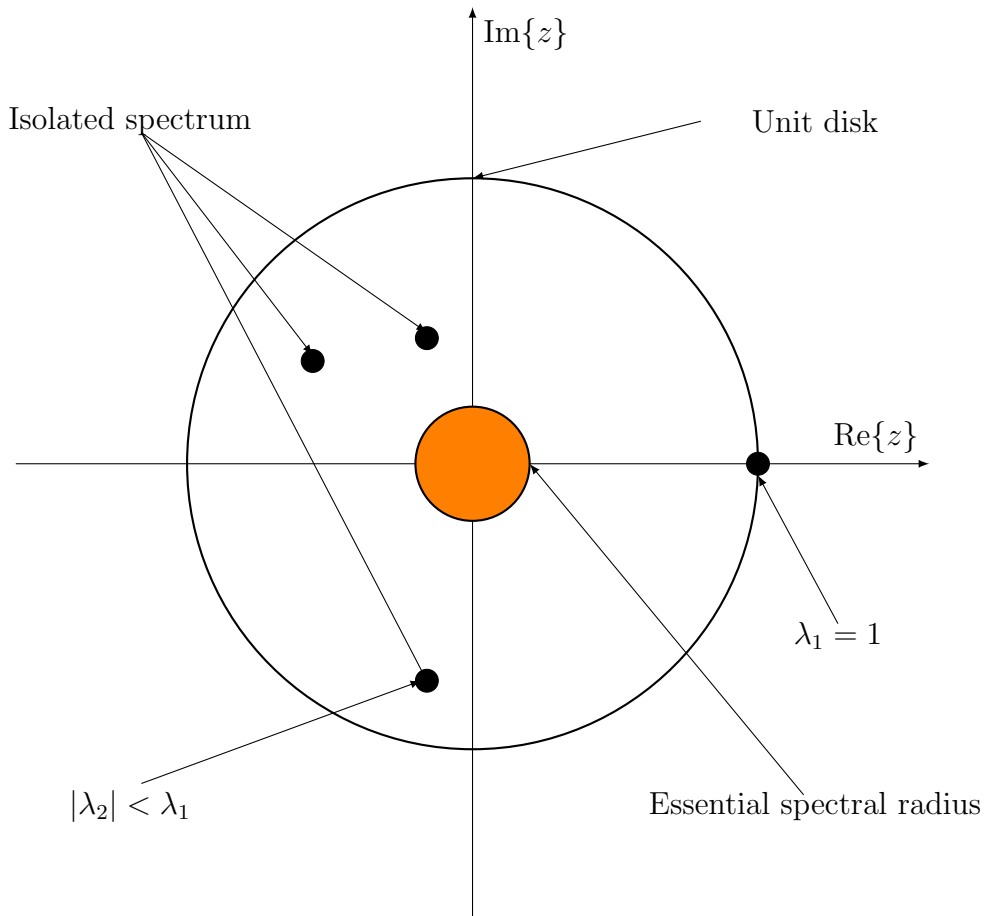


Figure 2.6: Spectrum of a stochastic matrix in the complex plane. The second eigenvalue, λ_2 describes the geometric convergence of the power method.

The authors of this paper identified that eigenvalues within the essential spectral radius corresponded to local features of a dynamical system while the isolated eigen-

¹⁸Some readers in other mathematical disciplines may call this the *spectral gap*.

¹⁹The algebraic multiplicity refers to repeated roots in the characteristic polynomials of an eigenvalue λ while the geometric multiplicity refers to the maximal number of linearly independent eigenvectors corresponding to λ . If these two values coincide, λ is called diagonalisable (or semi-simple) and the algebraic multiplicity is always greater than or equal to the geometric multiplicity.

values were related to the global features. Since then, research (both theoretical and numerical) has been motivated by the spectral-theoretic approach to transfer operators. In particular, they consider piecewise expanding C^2 transformations $T : [0, 1] \rightarrow [0, 1]$ and present a case study on the four-legs map. This is defined for $t \in \mathbb{R}$ as follows:

$$T_t(x) = \begin{cases} 2x & 0 \leq x < 1/4 \\ t(x - 1/4) & 1/4 \leq x < 1/2 \\ t(x - 3/4) + 1 & 1/2 \leq x < 3/4 \\ 2(x - 1) + 1 & 3/4 \leq x \leq 1. \end{cases} \quad (2.4.1)$$

We note that T_t is piecewise linear and has four branches; two with slope 2 and two with slope t . A typical graph of $T_t(x)$ with $t = 31/8$ is shown in the figure below.

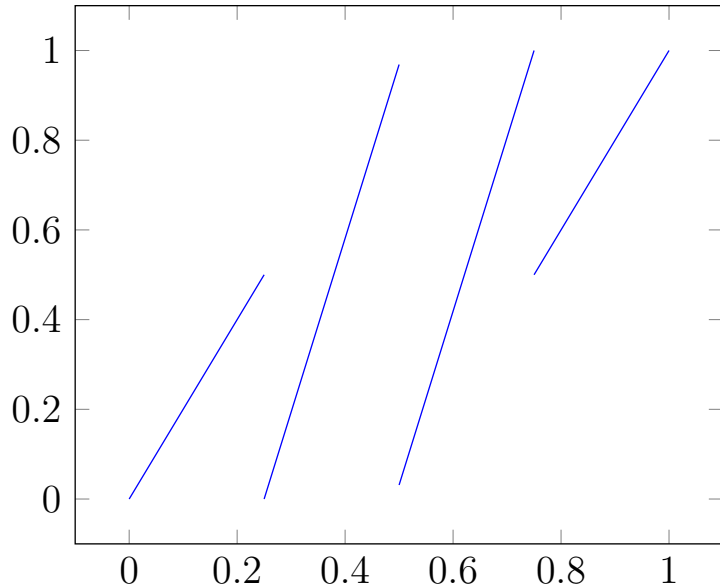


Figure 2.7: Graph of T_t for $t = 31/8$.

In particular, they study the spectral properties of the four-legs map for $2 \leq t \leq 4$; with a focus on values of t close to 4. We know from (2.2.11), and in particular, extending this result so

$$R_\sigma(\mathcal{P}|_{\mathcal{V}/\mathcal{N}}) \leq R_e \quad \text{and} \quad \{z \in \sigma(\mathcal{P}) : |z| > \sigma_e\} = \{z \in \sigma(\mathcal{P}|_{\mathcal{N}}) : |z| > \sigma_e\},$$

and thus, for all $t \in [2, 4]$, the essential spectrum of the Frobenius–Perron operator $\mathcal{P} : \mathcal{V} \rightarrow \mathcal{V}$ is contained inside $|z| \leq 1/2$.

Case 1: $t = 4$

The authors start by recognising that the map T_4 has a Markov partition given by the piecewise bounds for x , i.e.,

$$\mathfrak{M} = \{[0, 1/4], [1/4, 1/2], [1/2, 3/4], [3/4, 1]\}$$

is our Markov partition. Then by restricting the transfer operator to the four-dimensional space of piecewise-constant functions on \mathfrak{M} , they obtain the matrix representation (un-

der left multiplication):

$$\mathcal{P}_4 = \begin{pmatrix} 1/2 & 1/2 & 0 & 0 \\ 1/4 & 1/4 & 1/4 & 1/4 \\ 1/4 & 1/4 & 1/4 & 1/4 \\ 0 & 0 & 1/2 & 1/2 \end{pmatrix}.$$

Evidently we have eigenvalues $\lambda = 1, 1/2, 0$, and one can verify that a vector of ones $\varphi_4 = 1$ is the invariant density. Furthermore, we have for $\lambda = 1/2$, the eigenfunction

$$\psi_4 = \begin{cases} +1 & 0 \leq x < 1/2 \\ -1 & 1/2 \leq x \leq 1. \end{cases}$$

They showed that \mathcal{P}_4 has no spectral points outside of $|z| \leq 1/2$ barring the eigenvalue 1.

Case 2: $t < 4$

When $t < 4$, they construct a Markov partition by choosing t such that $T_t(1/2)$ from the third branch is mapped onto $x = 1/2$ after a finite number of iterations so that $T_t(1/2) \in [0, 1/4]$ for all $1 \leq k \leq n$. More specifically, they required that

$$T_t(1/2) = t(1/2 - 3/4) + 1 = 1/2^{n+1}$$

for any select $n \geq 1$. Solving for t_n gives

$$t_n = 4 - 1/2^{n-1},$$

which yields Markov partitions \mathfrak{M} of cardinality $2(n+1)$. As before, the Frobenius–Perron operator on t_n , denoted by $\mathcal{P}_{t_n} = P_n$ is restricted to piecewise-constant functions on the sets

$$\begin{aligned} &[0, 1/2^{n+1}], [1/2^{n+1}, 1/2^n], [1/2^n, 1/2^{n-1}], \dots, [1/4, 1/2] \\ &[1/2, 3/4], \dots, [1 - 1/2^n, 1 - 1/2^{n+1}], [1 - 1/2^{n+1}, 1]. \end{aligned}$$

Eigenvalues can be computed numerically, and they observed that there is a single real eigenvalue that moves from near 1 towards 1/2 (along the real line) as $n \rightarrow \infty$ and hence as $t_n \rightarrow 4$. In fact they also proved the following lemma:

Lemma 2.4.1. The matrix P_n has (only) one real eigenvalue λ_n in the interval

$$\left[\frac{1}{2} + \frac{1}{5n}, \frac{1}{2} + \frac{1}{n^{2/3}} \right]$$

and no other real eigenvalues in $[1/2, 1]$.

From here, they proceed to generalise these results to piecewise maps. We will describe one of the methods for producing an isolated eigenvalue:

1. Consider a mixing piecewise-linear Markov map T with k linear branches whose Frobenius–Perron operator \mathcal{P} has an eigenvalue $0 < \lambda < 1$.
2. Suppose that $|\lambda| < R_e$. For each $i = 1, \dots, k$, replace the i th branch of the map T (denote this by T_i) by l smaller branches $\tilde{T}_{i_1}, \dots, \tilde{T}_{i_l}$ that have slope $l|T'_i|$ in which the image of each \tilde{T}_{i_j} , $j = 1, \dots, l$ is equal to the image of T_i .
3. Setting $\tilde{\mathcal{P}}$ and \tilde{R}_e to be the Frobenius–Perron operator and essential spectral radius bound for \tilde{T} , we then have that $\tilde{R}_e = R_e/l$. It is also true that λ is still an eigenvalue for $\tilde{\mathcal{P}}$ and by marking l large enough, the essential spectral radius may be shrunk so that λ lies outside it.

2.4.2 Detecting Isolated Spectrum of Transfer and Composition Operators with Harmonic Analysis

Following on from the so-called Dellnitz–Froyland ansatz; Froyland, González-Tokman, and Quas use a harmonic analytic approach based on recent stability results established in [3]. The results in this paper established that the Frobenius–Perron operator acting on fractional Sobolev spaces of the interval, $\mathcal{P} : \mathbb{W}^{s,p}(I) \rightarrow \mathbb{W}^{s,p}(I)$, is bounded²⁰. Using this result, they were able to prove stability of the Ulam scheme (discussed in the previous chapter) acting under a fractional Sobolev norm. Although it is possible to determine (sometimes explicitly) spectral properties of transfer operators such as estimates on the essential spectral radius, determining the number of isolated eigenvalues has not been addressed. The spectrum of an operator can range from finite, to countably infinite and in this paper, they discuss methods to detect said region of the spectrum, and apply these methods to both one and two dimensional systems. This transition between the essential and non-essential spectrum can be observed in relatively simple systems. Consider the piecewise expanding map with positive parameters $\delta, \varepsilon > 0$ given by

$$T(x) = \begin{cases} 2\left(1 + \frac{3\delta}{\sqrt{2}}\right)x & x \in [0, \frac{1}{6}) \\ \frac{1}{3} + \frac{\delta}{\sqrt{2}} - 2\left(1 + \frac{3\delta}{\sqrt{2}}\right)\left(x - \frac{1}{6}\right) + 1000\left(x - \frac{1}{6}\right)^2\left(x - \frac{1}{3}\right)^2 & x \in [\frac{1}{6}, \frac{1}{3}) \\ \frac{4}{9} + \left(2 + \frac{9\varepsilon}{\sqrt{2}}\right)\left(x - \frac{1}{3}\right) & x \in [\frac{1}{3}, \frac{4}{9}) \\ \frac{1}{2} - \left(3 + \frac{18\varepsilon}{\sqrt{2}}\right)\left(x - \frac{1}{2}\right) + 100000\left(x - \frac{4}{9}\right)^2\left(x - \frac{5}{9}\right)^3 & x \in [\frac{4}{9}, \frac{5}{9}) \\ \frac{1}{3} - \frac{\varepsilon}{\sqrt{2}} + \left(2 + \frac{9\varepsilon}{\sqrt{2}}\right)\left(x - \frac{5}{9}\right) & x \in [\frac{5}{9}, \frac{2}{3}) \\ 1 - 2\left(1 + \frac{3\varepsilon}{\sqrt{2}}\right)\left(x - \frac{2}{3}\right) & x \in [\frac{2}{3}, \frac{5}{6}) \\ 1 + 2\left(1 + \frac{3\varepsilon}{\sqrt{2}}\right)\left(x - 1\right) & x \in [\frac{5}{6}, 1) \end{cases}. \quad (2.4.2)$$

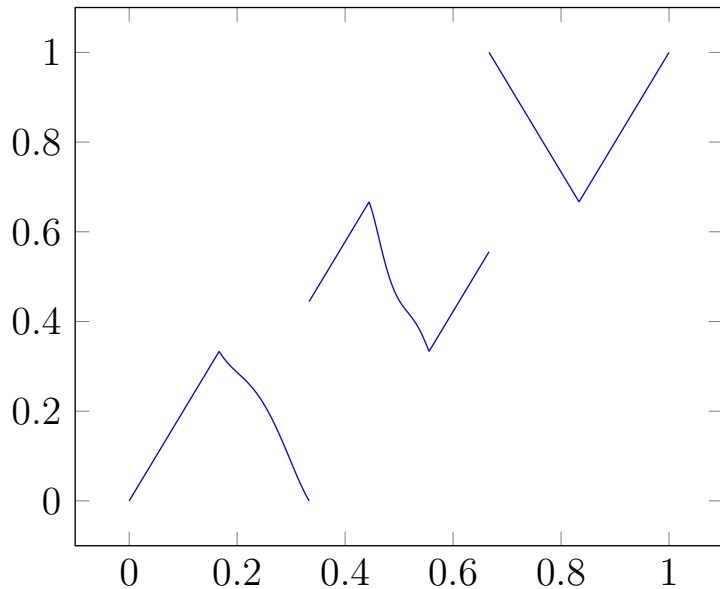
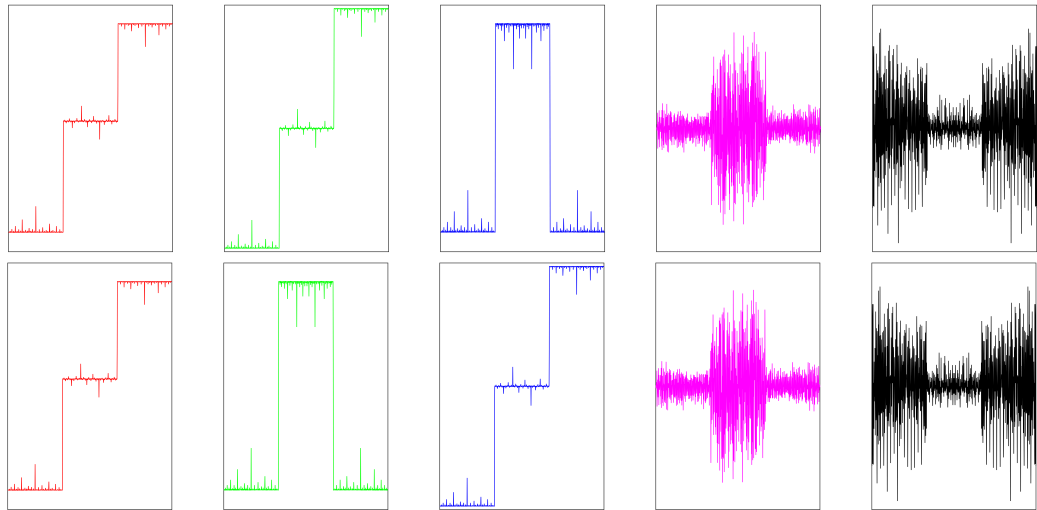


Figure 2.8: The map given by equation (2.4.2) with parameters $\varepsilon = 0$ and $\delta = 0$.

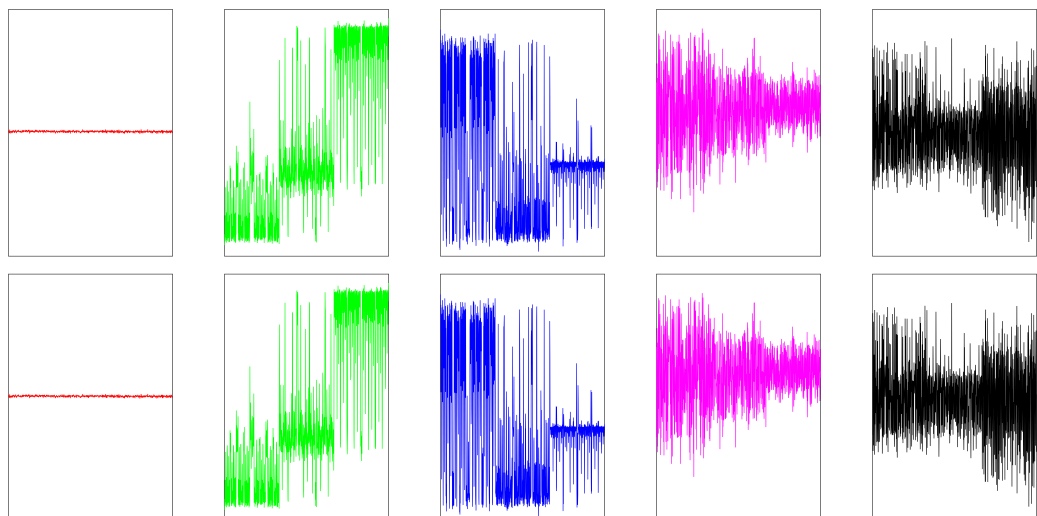
²⁰We remind the reader that a linear operator $\mathcal{L} : \mathbb{X} \rightarrow \mathbb{Y}$ from a vector space \mathbb{X} to another vector space \mathbb{Y} is *bounded* if for some constant $C > 0$, there holds for any element \vec{v} of the vector space, $\|\mathcal{L}\vec{v}\|_{\mathbb{Y}} \leq M\|\vec{v}\|_{\mathbb{X}}$.

2.4. LITERATURE REVIEW

When $\delta = \varepsilon = 0$, it is straightforward to distinguish the first three eigenvectors from the rest of the spectrum and identify the three invariant regions from the first three Koopman eigenvectors (see figures below). However, with a slight perturbation, $\delta > 0$ and $\varepsilon > 0$, the only (Lebesgue) invariant set becomes the unit interval and we are now left with three almost-invariant sets. This is observed in the left and right eigenvectors, in which we observe that the first three are fairly regular while the remaining two are quite noisy. In the perturbed case below (on page 32), we can see that there is now a noticeable separation between the three isolated eigenvalues and the eigenvectors have changed significantly (in particular, compare the noise in the 2nd and third eigenvectors from the perturbed and unperturbed dynamical systems). In addition to this, figure 2.10 shows the spectrum of the Koopman operator. The first shows the unperturbed case, where the three isolated eigenvalues are all close to 1. On the other hand, the perturbed system shows a significant separation between these three as well as a decrease in the spectral gap.

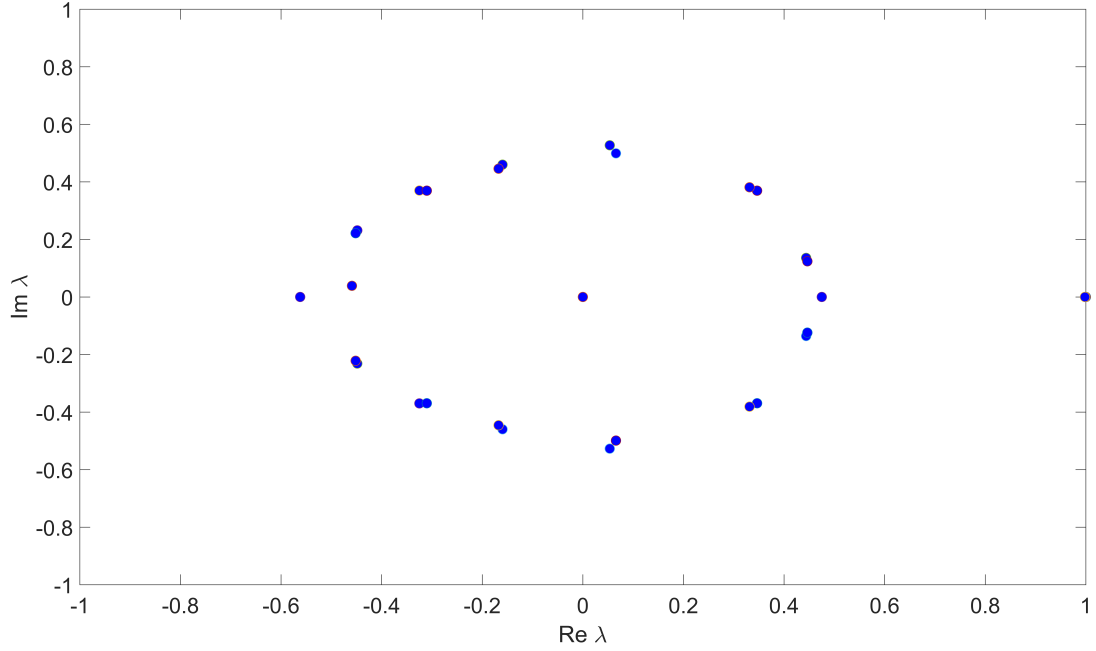


(a) The top row corresponds to the first five right eigenvectors while the bottom row to the first five left eigenvectors.

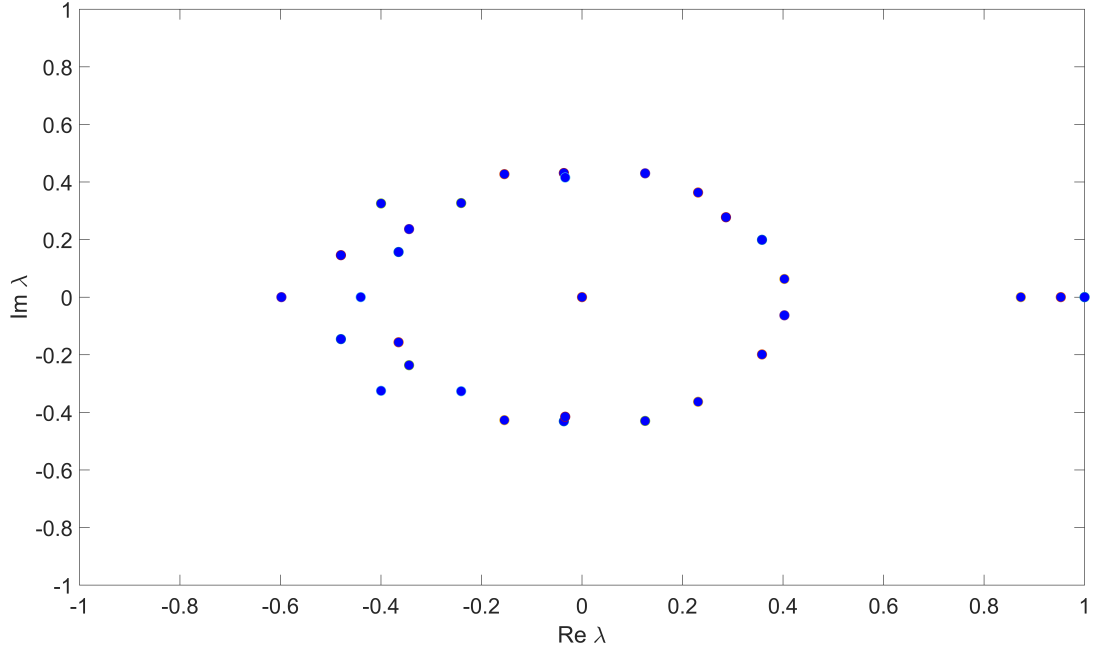


(b) As above, the top row corresponds to the right eigenvectors and the bottom the left but for the perturbed system, $\varepsilon = 0.01$ and $\delta = 0.0275$.

Figure 2.9: A comparison of the left and right eigenvectors of the dynamical system given by (2.4.2) .



(a) For the unperturbed system ($\varepsilon = \delta = 0$), one can see a clear separation between the isolated and non-isolated eigenvalues.



(b) For the perturbed system ($\varepsilon = 0.01$ and $\delta = 0.0275$), there is now a visible separation between the three isolated eigenvalues.

Figure 2.10: A comparison of the unperturbed and perturbed spectrum of the Koopman operator.

Given the stability of Koopman eigenvectors, the authors opt to work with the composition operator as opposed to the Frobenius–Perron operator. This allows them to exploit the quasi-compactness of the Koopman operator, but comes at the cost of treating it as a linear operator on a space of distributions. Prior to this paper, no rigorous results were established on the convergence of the Ulam scheme in *fractional*

2.4. LITERATURE REVIEW

*Sobolev spaces*²¹ — that is, a function $f(x) \in \mathbb{W}^{s,p}(\mathbb{X})$ is said to be an element of the fractional Sobolev space with (non-integer) parameter $s \in (0, 1)$ and $p \in [1, \infty]$ if

$$\mathbb{W}^{s,p}(\mathbb{X}) = \left\{ f(x) \in L^p(\mathbb{X}) : \frac{|f(x) - f(y)|}{|x - y|^{\frac{n}{p}+s}} \in L^p(\mathbb{X} \times \mathbb{X}) \right\}, \quad (2.4.3)$$

and is endowed with the norm²²

$$\|f(x)\|_{s,p} \equiv \left(\int_{\mathbb{X}} |f(x)|^p dx + \int_{\mathbb{X}} \int_{\mathbb{X}} \frac{|f(x) - f(y)|^p}{|x - y|^{n+sp}} dx dy \right)^{1/p}. \quad (2.4.4)$$

Although this form is commonly used in PDE literature (see [22]), numerically, it is more sensible to work with an equivalent formulation in terms of the Fourier transform. In particular, if one denotes the *n-dimensional Fourier transform* of $f(x)$ by

$$\mathcal{F}f(x) = \widehat{f}(\xi) = \frac{1}{(2\pi)^{n/2}} \int_{\mathbb{R}^n} f(x) e^{-i\xi \cdot x} dx \quad (2.4.5)$$

and the inverse by

$$\mathcal{F}^{-1}\widehat{f}(\xi) = f(x) = \frac{1}{(2\pi)^{n/2}} \int_{\mathbb{R}^n} \widehat{f}(\xi) e^{-i\xi \cdot x} d\xi,$$

then an equivalent statement to (2.4.4) is

$$\mathcal{F}^{-1}((1 + |\xi|^2)^{s/2} \widehat{f}(\xi)) \in L^p(\mathbb{X}). \quad (2.4.6)$$

This function space, also called the *space of Bessel potentials*, is much more useful as very efficient routines exist for computing the Discrete Fourier transform (DFT) of a vector. As was previously mentioned, such spaces traditionally arise in potential theory and PDEs, but in [24], they discuss these in the context of “mix-norms”, norms that measure mixing in a dynamical system. The parameter s in (2.4.6) is a smoothing parameter, which is related to the smoothness of the function, in particular, it cannot be larger than the smoothness of the derivative of the map. Using results established in [3], Froyland, González-Tokman, and Quas were able to prove the following theorem:

Theorem 2.4.2 (Convergence of the Ulam scheme in fractional Sobolev spaces). *Let $0 < \alpha \leq 1$, $0 < s' < s < \min\{\alpha, 1/p\} < 1$, $T : I \curvearrowright$ a piecewise $C^{1+\alpha}(\mathbb{X})$ a sufficiently expanding map, and $\mathcal{P} : \mathbb{W}^{s,p}(\mathbb{X}) \curvearrowright$ be the Frobenius–Perron operator of T . Then given the sequence of approximations to the Frobenius–Perron operator, $\{\mathcal{P}_n\}_{n=1}^\infty$ with n subintervals of uniform length, $\varepsilon_n \equiv 1/n$, the stability result of Keller–Liverani holds. In particular, the isolated eigenvalues and eigenspaces of \mathcal{P}_n and \mathcal{K}_n converge in $\mathbb{W}^{s',p}(\mathbb{X})$ and $(\mathbb{W}^{s',p}(\mathbb{X}))^* = \mathbb{W}^{-s',p}(\mathbb{X})$ respectively, to those of their corresponding Frobenius–Perron and Koopman operators.*

Note that even though the theorem is stated for intervals, it is simple enough to adapt to periodic functions, i.e., on the torus \mathbb{T} , as pointwise values are irrelevant for the function spaces they are studied on in this paper. From here, they use the fractional Sobolev norm defined by (2.4.6) to generate a smoothed approximation²³ to the original

²¹Sobolev spaces are commonly seen in the PDE literature, in particular, see [23] and [22].

²²The second term in this norm is called the *Gagliardo semi-norm*.

²³The idea of smoothed approximations is owed to analysis, in which one may convolve a discontinuous function with a C^∞ bump function to get a new function that is a smooth approximation of the discontinuous function.

2.4. LITERATURE REVIEW

eigenvectors. As there is an isometry between $\mathbb{W}^{s,p}(\mathbb{X})$ and $L^q(\mathbb{X})$, it is simple enough to use this after taking a discrete Fourier transform of the eigenvectors.

Given these results, they suggest the following algorithm (listed below) for numerically detecting the isolated spectrum of Frobenius–Perron and Koopman operators. The smoothing procedure is owed to the decaying term,

$$(1 + |\xi|^2)^{-s/2}$$

which can be thought of as penalising higher frequencies in the eigenvectors. They also include an optional weighting function,

$$\left(\frac{\sin(\pi\xi/N)}{\pi\xi N} \right)^2,$$

but note that there is little difference with or without it. Now since we have a smoothing operator in Fourier domain, inverting then suggests one should use a threshold, say τ , for discarding any remaining eigenvectors below said threshold as non-isolated spectrum. They proceed to test this procedure on a variety of 1 and 2 dimensional maps and different parameters, noting the efficacy of the approach.

Algorithm 3: Fourier threshold for isolated spectrum of transfer/composition operators.

Input : Number of boxes N , flow (resp. map) T and time step t (resp. n), constant K for sampling per box.

Output: Smoothed isolated eigenvectors of Froebnius–Perron/Koopman operators.

1 Set parameters

$$0 < s < 1/p < 1 \quad \text{and} \quad q = (1 - p^{-1})^{-1}.$$

- 2 Compute the Ulam matrix \hat{P} for flow/map T and top k right/Koopman eigenvectors $\{w_1, \dots, w_k\}$ of \hat{P} .
- 3 Compute their discrete Fourier transforms $\{\hat{w}_1, \dots, \hat{w}_k\}$.
- 4 Compute the weighted discrete Fourier transforms $z'_j(\xi) = \hat{w}_j(\xi)(1 + |\xi|^2)^{-s/2}$ and set $z_j(\xi) = z'_j(\xi) (\sin(\pi\xi/N)/(\pi\xi/N))^2$.
- 5 Compute the inverse discrete Fourier transforms $\{z_1, \dots, z_k\}$.
- 6 Set a threshold $\tau > 0$.
- 7 **if** $\|z_j\|_{L^q} < \tau$ **then**
- 8 | Discard w_l as an isolated eigenvector for all $l \geq j$.
- 9 **end**

Given this algorithm, we will see in the following chapter a wavelet equivalent for detecting the isolated spectrum of transfer operators.

Chapter 3

A Wavelet Approach to the Spectrum of Transfer Operators

3.1 Wavelet Theory

In order to proceed with the wavelet collocation method, some basic facts of harmonic analysis are recalled from [21] and [18].

Definition 3.1.1 (Wavelet transform). The *continuous wavelet transform* of $f(x) \in L^2(\mathbb{R})$ at scale t and position u is given by the integral inner product, defined as

$$\mathcal{W}_\psi f(u, t) = \langle f(x), \psi_{u,t}(x) \rangle = \int_{\mathbb{R}} f(x) \psi_{u,t}(x) dx = \int_{\mathbb{R}} f(x) \frac{1}{\sqrt{|t|}} \psi^* \left(\frac{x-u}{t} \right) dx,$$

where $t \neq 0$, $x, u \in \mathbb{R}$, and $\psi_{u,t} \in L^2(\mathbb{R})$ is the wavelet, with mother wavelet $\psi(x)$.

The mother wavelet $\psi(x)$ plays the same role as the kernel in the Fourier transform but with one major difference, ψ is non-unique. Now since the kernel of the wavelet transform is non-unique, it is sometimes possible to define multiple inverse wavelet transforms. However, it is still required to restrict this set of inverse formulæ. Hence we introduce:

Definition 3.1.2 (Calderón's admissibility condition). The *Calderón admissibility condition* states that in order to have a well-defined inverse transform for a given wavelet $\psi(x)$, it is required that

$$C_\psi = \int_{\mathbb{R}} \frac{|\widehat{\psi}(\xi)|^2}{|\xi|} d\xi < \infty.$$

Wavelets that satisfy this condition are sometimes called *continuum wavelets*.

Carefully note that the Calderón admissibility condition does not imply localisation in both time and frequency domains. It does however, imply that the average value of the wavelet must be zero¹.

Theorem 3.1.3 (Wavelet inversion formula). *Suppose that $\psi(x)$ is a continuum wavelet which is also normalised in the Calderón admissibility condition, i.e., $C_\psi = 1$. Then for any $f(x) \in L^2(\mathbb{R})$, we have the $L^2(\mathbb{R})$ inversion formula,*

$$f(x) = \int_{\mathbb{R}^2} \frac{\mathcal{W}_\psi f(u, t)}{\sqrt{|t|}} \psi_{u,t}(x) \frac{du dt}{t^2} = \lim_{\substack{\varepsilon \rightarrow 0, \\ A, B \rightarrow \infty}} \int_{\substack{\varepsilon < |t| < A, \\ |u| < B}} \frac{\mathcal{W}_\psi f(u, t)}{\sqrt{|t|}} \psi_{u,t}^*(x) \frac{du dt}{t^2},$$

where one interprets the integral above as a Cauchy principal value.

¹Some texts on harmonic analysis use this definition for a wavelet instead.

Note that we can normalise the above inversion formula simply by dividing by C_ψ . Given that wavelets were first rigorously treated in harmonic analysis, naturally there are a large number of results concerning the regularity of wavelets and upper/lower bounds on coefficients in wavelet series/transforms. Although these results are not the primary focus for the development of this algorithm we will make use of certain definitions to gain insight into how the algorithm acts with different wavelets. One such property we are interested in is:

Definition 3.1.4 (Vanishing moments). A function $f(x) : \Omega \rightarrow \mathbb{R}$ is said to have n vanishing moments if

$$\int_{\mathbb{R}} x^k f(x) dx = 0 \quad (3.1.1)$$

for $0 \leq k < n \in \mathbb{N}$.

Those familiar with orthogonal polynomials may recognise this in the context that a polynomial with n vanishing moments is orthogonal to a polynomial of degree $n - 1$.

Definition 3.1.5 (Frame, Riesz Basis). Given a Hilbert space \mathcal{H} , we call the sequence $\{\varphi_n\}_{n \in \Gamma}$ where Γ is a potentially infinite indexed subset of the integers, a *frame* if there are two constants $0 < A \leq B$ such that for every function $f(x) \in \mathcal{H}$,

$$A\|f(x)\|^2 \leq \sum_{n \in \Gamma} |\langle f(x), \varphi_n \rangle|^2 \leq B\|f(x)\|^2.$$

When $A = B$, the frame is called *tight*, and if the $\{\varphi_n\}_{n \in \Gamma}$ are linearly independent, then the frame is called a *Riesz basis*. If $A = B = 1$, then this is simply an orthonormal system.

Note that from here onward, we will be referring to discrete wavelet analysis as well, and thus when appropriate, t and u are replaced by j and k respectively.

Definition 3.1.6 (Multiresolution Analysis). We call an increasing sequence of closed subspaces $\{V_j\}_{j \in \mathbb{Z}} \subset L^2(\mathbb{R})$ a *multiresolution analysis* if there exists a function Φ (called the *scaling function*) such that $\{\Phi(x - n)\}_{n \in \mathbb{Z}}$ is a Riesz basis of V_0 and the following hold:

- (i) For all $j, k \in \mathbb{Z}$, then $f(x) \in V_j$ if and only if $f(x - 2^j) \in V_k$;
- (ii) For all $j \in \mathbb{Z}$, $V_{j+1} \subset V_j$;
- (iii) For all $j \in \mathbb{Z}$, $f(x) \in V_j$ if and only if $f(x/2) \in V_{j+1}$;
- (iv) $\lim_{j \rightarrow +\infty} V_j = \bigcap_{j \in \mathbb{Z}} V_j = \{0\}$; and
- (v) $\lim_{j \rightarrow -\infty} V_j = \text{closure} \left(\bigcup_{j \in \mathbb{Z}} V_j \right) = L^2(\mathbb{R})$.

Remark 3.1.7. Multiresolution analysis is used in the study of orthogonal wavelets and in particular, is used to help construct wavelets and appropriate scaling functions. All of the wavelets utilised in the numerical experiments have the multiresolution property. It is important to note that more general wavelets exist, such as *biorthogonal* or *second generation wavelets*, which do not have the multiresolution analysis property. These wavelets will not be discussed beyond this remark.

3.2 The Algorithm

A new algorithm is proposed as an alternative to ‘‘Test 1’’, i.e., Algorithm 2 from [11], which makes use of the wavelet characterisation of fractional Sobolev spaces. In order to describe this algorithm, we recall a proposition from [21]:

Proposition 3.2.1. Suppose that ψ is a normalised continuum wavelet and

$$C_{\psi,s} \equiv \int_{\mathbb{R}} \frac{|\widehat{\psi}(\xi)|^2}{|\xi|^{1+2s}} d\xi < \infty$$

holds for some $s > 0$. Then the fractional Sobolev norm of $f(x) \in L^2(\mathbb{R})$ measured by

$$\|f(x)\|_{2,s}^2 = \int_{\mathbb{R}} |\xi|^{2s} |\widehat{f}(\xi)|^2 d\xi$$

is equivalent to a weighted $L^2(\mathbb{X})$ norm of the wavelet transform,

$$\int_{\mathbb{R}} \int_{\mathbb{R}} |\mathcal{W}_{\psi} f(u, t)|^2 \frac{du dt}{|u|^{2(1+s)}} = C_{\psi,s} \|f(x)\|_{2,s}^2. \quad (3.2.1)$$

Although one may be tempted to implement this directly, first observe that there are three integrals to evaluate with two of them containing singularities in the integrand (and over the region of integration). However, there is another equivalent representation of a wavelet norm in the fractional Sobolev space $\mathbb{W}^{s,2}(\mathbb{X})$, which is given by (see [5])

$$f(x) \in \mathbb{W}^{s,2}(\mathbb{X}) \Leftrightarrow \sum_{j,k} |\langle f(x), \psi_{j,k}(x) \rangle|^2 (1 + 2^{-2js}) < \infty, \quad (3.2.2)$$

where j and k range over all (discrete) scales and translations respectively. Instead of evaluating (3.2.1), the norm given by (3.2.2) is much more sensible to implement numerically. For the numerical algorithm, to create better separation between higher and lower scales, the following will be used for Frobenius–Perron eigenvectors:

$$f(x) \in \mathbb{W}^{s,2}(\mathbb{X}) \Leftrightarrow \|f(x)\|_{s,2} = \left(\sum_{j,k} |\langle f(x), \psi_{j,k}(x) \rangle|^2 2^{-2js} \right)^{1/2} < \infty. \quad (3.2.3)$$

Similarly for the dual space, the Koopman eigenvector norms will be computed as

$$g(x) \in \mathbb{W}^{-s,2}(\mathbb{X}) \Leftrightarrow \|g(x)\|_{-s,2} = \left(\sum_{j,k} |\langle g(x), \psi_{j,k}(x) \rangle|^2 2^{2js} \right)^{1/2}. \quad (3.2.4)$$

These were shown to be equivalent norms by Meyer in [19]. Note however, that these norms are for one dimension only. In higher dimensions, a tensor product construction may be used and scale and translation indices j and k become multi-indices, $j = (j_1, \dots, j_d)$ and (k_1, \dots, k_d) for d -dimensional spaces. In addition, an angle parameter θ may be introduced, in which one may rotate the wavelet in the physical space. For radially symmetric wavelets such as the Mexican hat wavelet, this does not affect the coefficients. This angle however, will be restricted to $\theta = 0$ for all numerical experiments. Furthermore, (3.2.2) assumes square integrability of $f(x)$ as indicated by

the 2 in the superscript and the use of the inner product in the norms above. The numerical tests to follow will be restricted to this case².

Algorithm 4: Wavelet threshold for isolated spectrum of transfer/composition operators.

Input : Number of boxes N , flow (resp. map) T and time step t , constant K for sampling per box.

Output: Smoothed eigenvectors w_l of the Koopman/Frobenius–Perron operators and their fractional Sobolev norms.

- 1 Set $0 < s < 1/p < 1$ ($q = 2$).
- 2 Compute the Ulam matrix \hat{P} for flow/map T and top m right/Koopman eigenvectors $\{w_1, \dots, w_m\}$ of \hat{P} .
- 3 Compute the continuous wavelet transform of each eigenvector, $\{\mathcal{W}_\psi w_1, \dots, \mathcal{W}_\psi w_m\}$.
- 4 For each eigenvector, compute the fractional Sobolev norm according to

$$\|f(x)\|_{2,s} = \sum_{j,k} |\langle f(x), \psi_{j,k}(x) \rangle|^2 2^{-2js}.$$

- 5 Set threshold $\tau > 0$.
- 6 **if** $\|\mathcal{W}_\psi w_m\|_{2,s} < \tau$ **then**
- 7 | Discard w_l as an isolated eigenvector for all $l \geq m$.
- 8 **end**

Note that there is no set way to compute or choose the threshold τ here, although one can be given more freedom if the wavelet has similar regularity and correlation with the dynamical system itself. This is further discussed in the numerical experiments below. In particular, this phenomenon will be observed in the spectral gap between the isolated and non-isolated spectrum of the Frobenius–Perron and Koopman operators.

3.2.1 Numerical Experiments

When choosing a wavelet, one may wish to optimise a particular property that corresponds to certain factors, such as data compression, noise removal or fast calculations. This corresponds to using a particular wavelet with few non-zero coefficients $\langle f(x), \psi_{u,t}(x) \rangle$. It is a well-known fact in wavelet literature that a function $f(x)$ has few non-negligible wavelet coefficients if the high-resolution, or fine-scale coefficients are small. It has been proven that this is dependent on a combination of mathematical properties such as the regularity of $f(x)$, the number of vanishing moments of ψ , and the size of the support. Here, we summarise the different wavelets used and also list some of their properties:

- **Haar:** The Haar wavelet was first introduced in 1910 by Alfred Haar when he was searching for a discontinuous orthonormal basis for $L^2([0, 1])$. The Haar wavelet

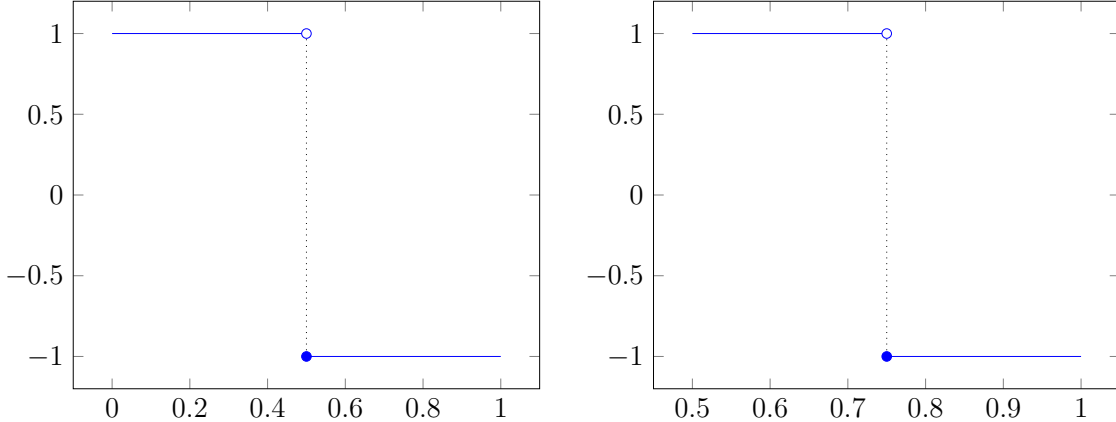
²Some theory of wavelets has been developed in other function spaces, although these will not be considered.

3.2. THE ALGORITHM

is given by

$$\psi(x) = \begin{cases} +1 & x \in [0, 1/2), \\ -1 & x \in [1/2, 1), \\ 0 & \text{otherwise.} \end{cases}$$

It has $n = 1$ vanishing moments and compact support.



(a) The mother wavelet for the Haar function, $\psi_{1,0}(x) = \psi(x)$. (b) The next level Haar wavelet with translation, $\psi_{2,1}(x) = \psi(2x - 1)$.

Figure 3.1: A visual demonstration of the multiscale/wavelet analysis. Here, one may think of scale related to “frequency” in the Fourier domain.

Note from the figure above, that the support decreases by a factor of 2 as the level of the scale increases.

- **Daubechies:** The Daubechies wavelet is quite unique. It does not have a closed form, has compact support, is orthogonal, and for n vanishing moments corresponds to n th order differentiability. The 0th order Daubechies wavelet does however, correspond to the Haar wavelet defined above.
- **Meyer:** The Meyer wavelet has infinite regularity, infinite support, symmetry, orthogonality and no explicit formulæ. Picking a function in the Schwartz class³, $g(x) \in \mathcal{S}(\mathbb{R})$ will produce a wavelet $\psi(x) \in \mathcal{S}(\mathbb{R})$:

- (i) $0 \leq g(\xi) \leq 1$ for all x ;
- (ii) $g(\xi) = g(-\xi)$ (symmetry);
- (iii) $g(\xi) = 1$, for $-2\pi/3 < |\xi| < 2\pi/3$;
- (iv) $\text{supp } g(\xi) \subset [-4\pi/3, 4\pi/3]$; and
- (v) $g(\xi)^2 + g(2\pi - \xi)^2 = 1$ for $0 < \xi < 2\pi$.

³Recall that this is the space of all functions whose derivatives are rapidly decreasing in the sense that $\mathcal{S}(\mathbb{R}^n) = \{f(x) \in C^\infty(\mathbb{R}^n) : \|f(x)\|_{\alpha,\beta} < \infty \forall \alpha, \beta \in \mathbb{Z}_+^n\}$ where $\|f(x)\|_{\alpha,\beta} = \sup_{x \in \mathbb{R}^n} |x^\alpha D^\beta f(x)|$ and multi-index notation is being used.

The wavelet used by MATLAB (and hence in the applications of this algorithm) are defined in the frequency domain,

$$\widehat{\psi}(\xi) = \begin{cases} \frac{1}{\sqrt{2\pi}} e^{i\xi/2} \sin\left(\frac{\pi}{2}\nu\left(\frac{3}{2\pi}|\xi| - 1\right)\right) & |\xi| \in \left[\frac{2\pi}{3}, \frac{4\pi}{3}\right] \\ \frac{1}{\sqrt{2\pi}} e^{i\xi/2} \cos\left(\frac{\pi}{2}\nu\left(\frac{3}{4\pi}|\xi| - 1\right)\right) & |\xi| \in \left[\frac{4\pi}{3}, \frac{8\pi}{3}\right], \\ 0 & |\xi| \notin \left[\frac{2\pi}{3}, \frac{8\pi}{3}\right] \end{cases}, \quad (3.2.5)$$

where

$$\nu(a) = a^4 (35 - 84a + 70a^2 - 20a^3), \quad a \in [0, 1] \quad (3.2.6)$$

and scaling function

$$\widehat{\varphi}(\xi) = \begin{cases} \frac{1}{\sqrt{2\pi}} & |\xi| \leq \frac{2\pi}{3} \\ \frac{1}{\sqrt{2\pi}} & |\xi| \in \left[\frac{2\pi}{3}, \frac{4\pi}{3}\right], \\ 0 & |\xi| > \frac{4\pi}{3} \end{cases}, \quad (3.2.7)$$

which as mentioned, does not have finite support, but does satisfy the following decay property for all $n \in \mathbb{N}$:

$$|\psi(x)| \leq C_n(1 + |x|^2)^{-n}$$

for some appropriately defined constant C_n (i.e., decays faster than any inverse polynomial). A similar property holds for its derivative.

- **Morlet/Gabor:** The Morlet, or Gabor wavelet, has non-compact support, symmetry, not orthogonal, infinite differentiability, and is defined by

$$\psi(x) = e^{-x^2/2} \cos(5x).$$

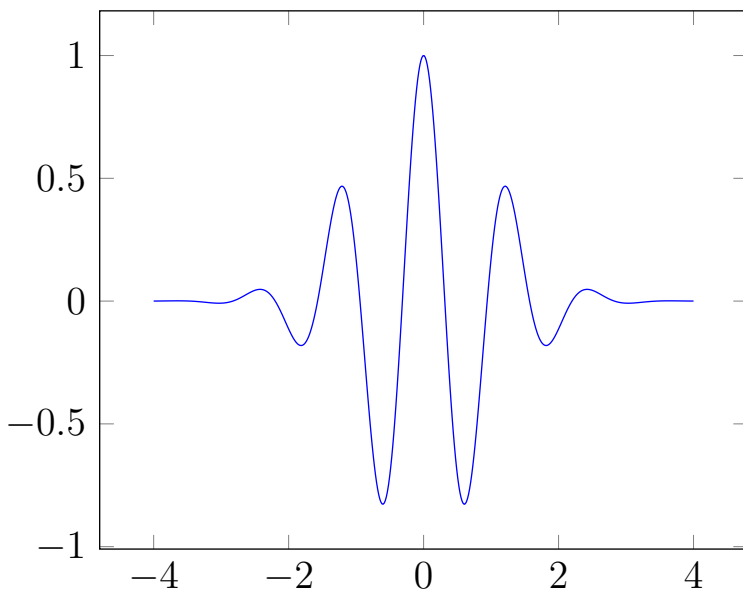


Figure 3.2: The Morlet/Gabor wavelet, $\psi(x) = \psi_{1,0}(x) = e^{-x^2/2} \cos(5x)$.

3.2. THE ALGORITHM

- **Mexican Hat/Ricker:** The Mexican hat or Ricker wavelet is defined through its Fourier transform,

$$\hat{\psi}(\xi) = C\xi^2 e^{-\pi\xi^2}$$

which one may recognise as the second derivative of the Gaussian. Here, $C > 0$ is a normalisation constant which is computed through the admissibility condition. This wavelet is non-orthogonal, symmetric and has infinite support.

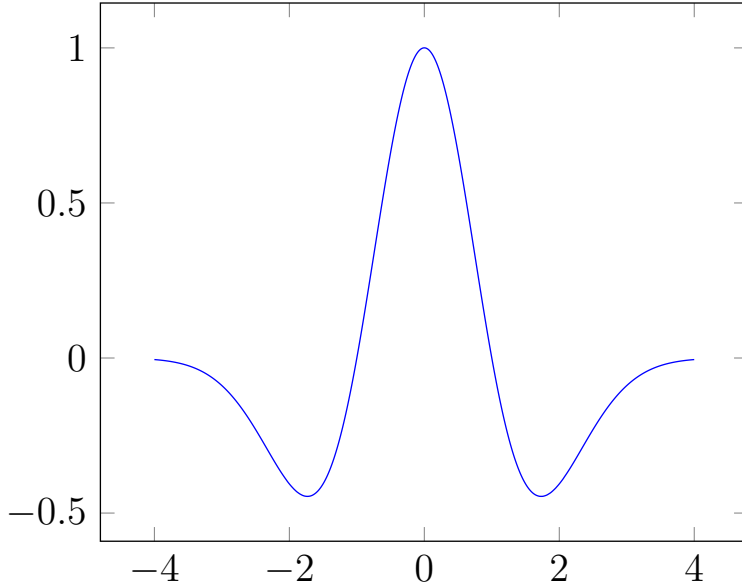


Figure 3.3: The Mexican hat wavelet, $\psi(x) = C(1 - x^2)e^{-x^2/2}$.

Note that this is by no means an exhaustive list of possible wavelets, only a subset which exhibit different properties. It is possible that more modern wavelets would achieve a different outcome to the results below.

With these in mind, we now present a series of numerical experiments that explore the application of this algorithm to a large class of models found in dynamical systems and ergodic theory.

A 1-D Map with Three Invariant Sets

We consider the same map 1-D discrete-time map used in [11] with a selection of values for the parameters ε and δ , which controls the height of the peaks, or the “size of the hole in the leak”. In summary, we consider three main experiments:

- (i) Fix ε, δ parameters in map, fix smoothness parameter s , and change wavelets;
- (ii) Fix smoothness parameter s and wavelet, change leakage parameters ε and δ ; and
- (iii) Fix wavelet basis, fix map parameters ε and δ , change smoothness parameter.

Experiment 1: Here, we fix $s = 0.4$, $\varepsilon = 0.001$, $\delta = 0.00275$ and consider the following wavelets:

- Haar;
- Daubechies 2 and 8;

3.2. THE ALGORITHM

- Meyer;
- Mexican hat; and
- Morlet.

The results for these are compared with the Fourier equivalent on both left and right eigenvectors. Referring to the figures below, the Haar wavelet has the least regularity and the corresponding norms in the figure directly below reflects this with a greater spectral gap between isolated and non-isolated eigenvalues, outperforming the Fourier algorithm. Comparing this with say the Meyer or Mexican hat wavelets which have infinite differentiability, the spectral gap is not as obvious. A medium can be observed in the Daubechies wavelets which have finite differentiability.

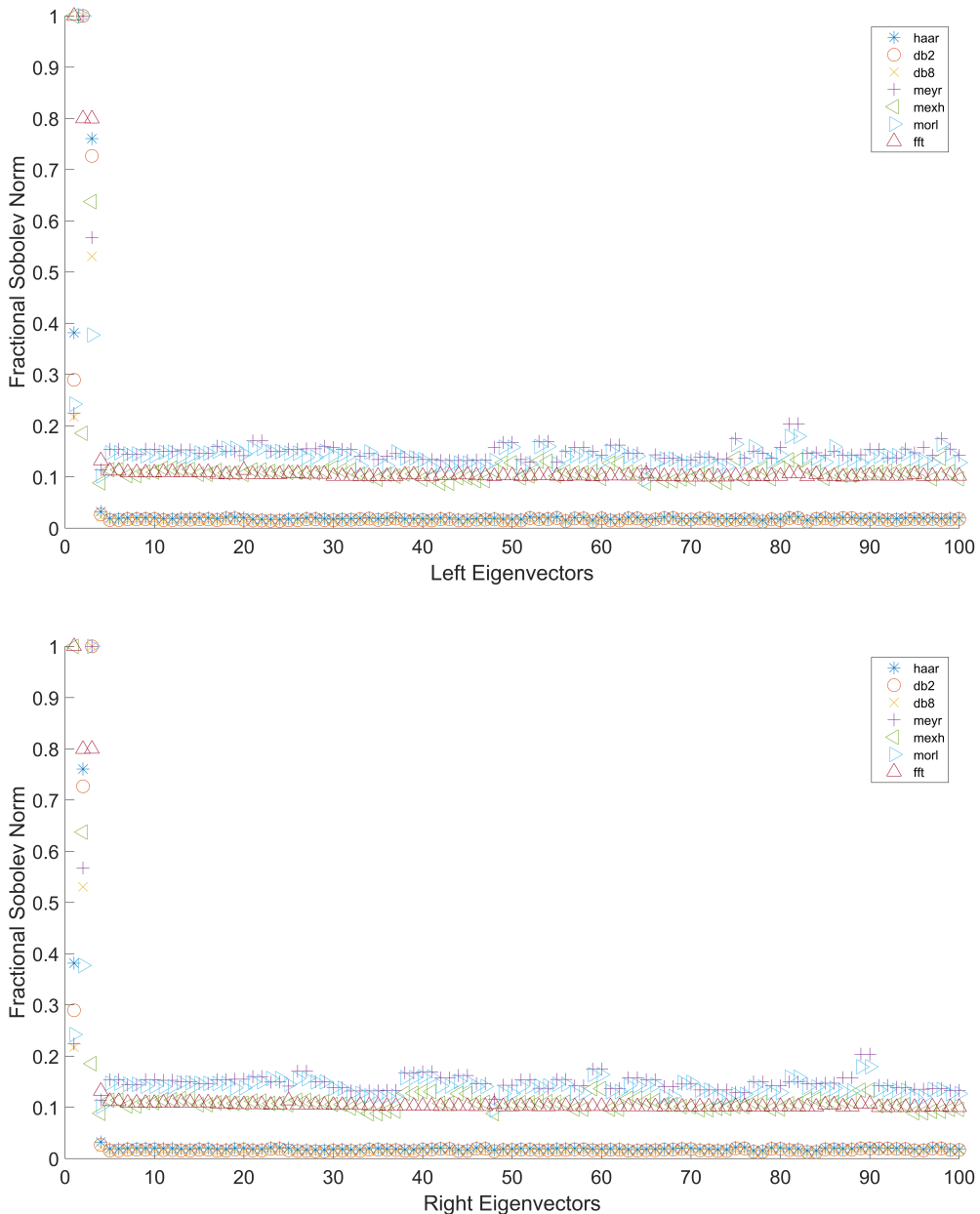


Figure 3.4: A plot of the eigenvectors and their fractional Sobolev norms under the six different wavelets and the Fourier basis.

3.2. THE ALGORITHM

Experiment 2: Now, we fix $s = 0.4$ as above along with a wavelet (we choose the Haar wavelet for this experiment) and perturb ε and δ . In particular, we choose $\delta = 0.25$ and $\varepsilon = 0.1$, which is significant enough to destroy one of the invariant sets, leaving only two elements of the isolated spectrum. As can be seen in the figure below, despite the perturbations from $\varepsilon = \delta = 0$, the spectral gap between isolated and non-isolated spectrum remains clear. In addition it can be observed that the Fourier algorithm is not as robust as the wavelet algorithm when considered with noise, as the spectral gap

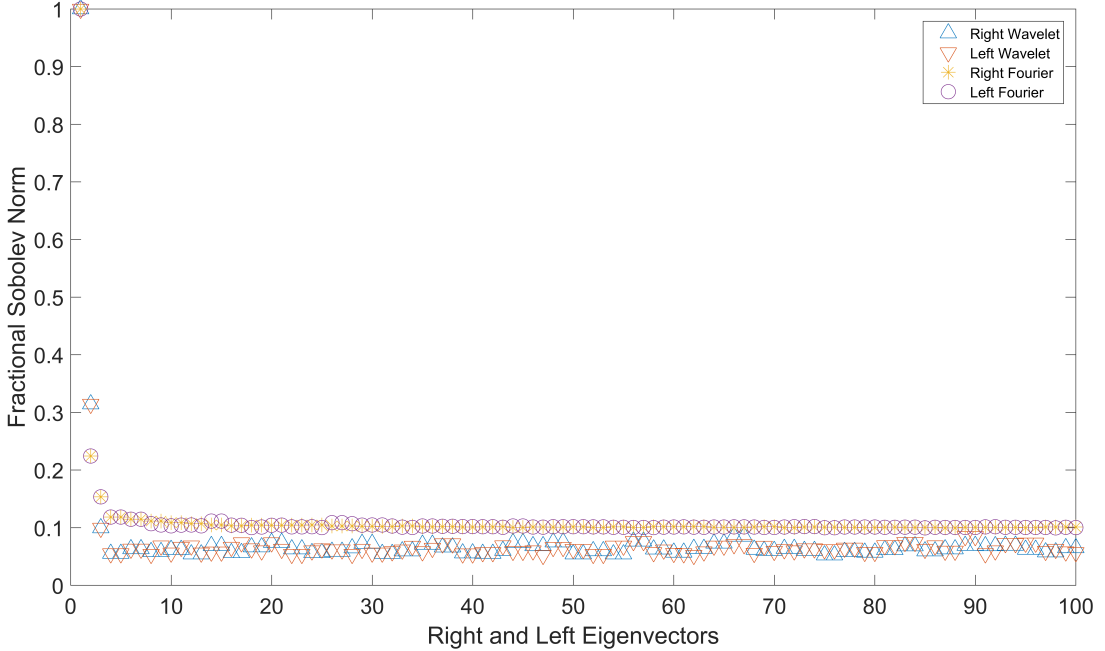


Figure 3.5: Left and right eigenvector norms for $\varepsilon = 0.1$ and $\delta = 0.25$.

Experiment 3: First, recall that since we are restricting to square-integrable functions, the smoothness parameter s should not exceed $1/p = 1/2$ in both algorithms since we do not have sufficient differentiability. The numerical instability of the wavelet algorithm becomes apparent as s exceeds this threshold, when all of the entries become NaNs due to numerical overflow. This can be observed by running the code in Appendix A.2 and setting s to be sufficiently larger than $1/2$.

The Quadruple-gyre

We consider the quadruple-gyre flow, a non-linear system of differential equations given by

$$\begin{cases} \dot{x} = -g(t, x, y) \\ \dot{y} = +g(t, y, x) \end{cases},$$

$$f(t, x) = \delta \sin(\omega t)x^2 + (1 - \delta \sin(\omega t))x,$$

$$\frac{\partial f}{\partial x} = \delta \sin(\omega t)x + 1 - \delta \sin(\omega t),$$

$$g(t, x, y) = \sin(A\pi f(t, x)) \cos(\pi f(t, y)) \frac{\partial f}{\partial x}(t, y),$$

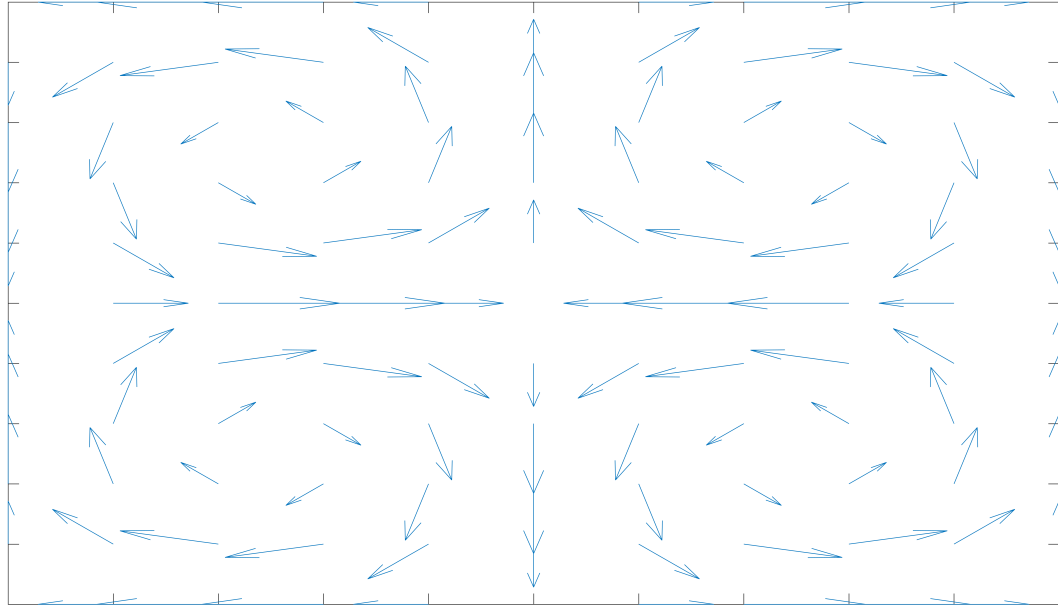
where δ , A , and ω are constants. This system was studied in [8] but we choose $\delta = 0.1$, $\omega = \pi/5$, and $A = 0.1$ instead and solve for one time step, i.e., step size of $h = 0.01$ and

3.2. THE ALGORITHM

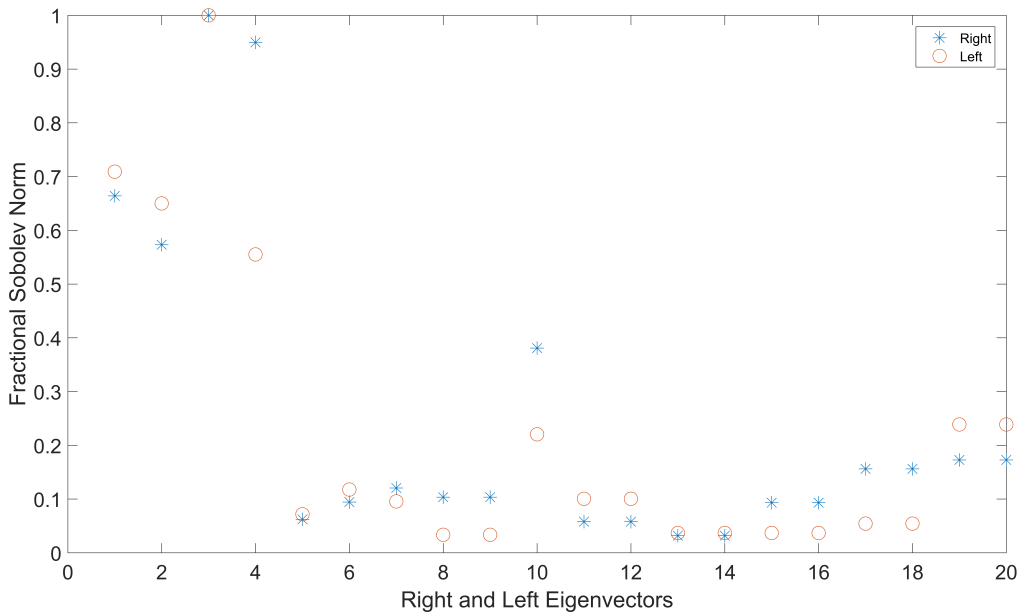
solve for $n = 100$ steps. A vector field plot is included at time $t = 0$. Refer to the final appendix for the code discussed here. As one would expect, the quadruple-gyre has four eddies, and this is reflected in the figures below, where the first four eigenvectors have a more significant wavelet fractional Sobolev norm than the rest of the spectrum. Here, $s = 1.5$ and a ‘sinc’ wavelet was used, explicitly given by

$$\widehat{\psi}(\xi_1, \xi_2) = [\text{sinc}(A_1(\xi_1 - \xi_{0,1})) \text{sinc}(A_2(\xi_2 - \xi_{0,2}))]^p, \\ A_1, A_2, \xi_{0,1}, \xi_{0,2} \in \mathbb{R}, p \in (0, \infty),$$

and was chosen due to the sinusoidal terms in both the wavelet and the quadruple-gyre system, as well as the sufficient differentiability. A threshold of 0.5 would work here to separate the isolated and non-isolated parts of the spectrum.



(a) The vector field for the quadruple-gyre at time $t = 0$.



(b) A plot of the right and left eigenvectors and their corresponding wavelet fractional Sobolev norms.

As a final note, it is not important that the fractional Sobolev norms of the eigenvec-

3.2. THE ALGORITHM

tors decrease monotonically, only that the norms of the eigenvectors with corresponding eigenvalues in the isolated spectrum have a significantly larger norm than the eigenvectors corresponding to eigenvalues of the non-isolated spectrum.

Overall, the above experiments have shown evidence that the wavelet basis can outperform the Fourier basis in terms of spectral separation if a suitable wavelet is chosen. The main drawback of this method however is the numerical instability when the smoothing parameter s becomes too high. Computational effort is similar for both of the algorithms but it is also infeasible to select a number of angles in 2-dimensional systems due to the size of the data.

Chapter 4

Discussion and Conclusions

A numerical study was conducted on a variety of maps and flows commonly found in dynamical systems. In addition to an exposition combining a variety of different areas of mathematics, both pure and applied, a numerical algorithm was developed using multi-scale analysis, i.e., wavelets. This algorithm can be used in conjunction with Ulam’s method to detect the number of slower than expected mixing sets, or in more practical terms, the number of eddies in some dynamical systems. It has also been demonstrated that if one knows a priori the regularity of the dynamical system (e.g., $C^\infty(\mathbb{X})$ for a smooth dynamical system versus $C^{1+\alpha}(\mathbb{X})$ for a map on the unit interval) then one can choose a corresponding wavelet with more or less regularity — which is related to the number of vanishing moments. Furthermore, the wavelet algorithm is more robust to noise when considering the spectral gap in the fractional Sobolev norms when compared to the Fourier equivalent. One caveat of the wavelet approach is the sensitivity to the smoothness of the dynamical system. When considering a dynamical system that is endowed with high regularity (e.g., the double-gyre), the smoothness parameter could be changed without affecting the stability of the algorithm. However, as was demonstrated on the 1-D map with three invariant sets (refer to Figure 2.8), this parameter is necessary for the stability, otherwise numerical overflow is possible. In addition to this, when considering higher dimensional wavelet transforms ($d \geq 2$), the size of the data increases significantly, as was mentioned that one has an angle parameter to rotate for 2-D wavelets. As the dimension (and degrees of freedom) increase, it is no longer feasible to consider directly using Ulam’s method and the wavelet algorithm. One potential solution to this is to consider a fully multi-scale library, using something akin to the “sparse Ulam method” discussed in [13]. This adaptation does not suffer as badly when the dimension and data increases.

Potential areas to expand upon this direction could include the analysis of more wavelets, including the so-called *2nd generation wavelets*, i.e., non-orthogonal wavelets. Non-orthogonal wavelets have the same advantages of the Daubechies wavelets, i.e., compact support and finite differentiability, but often have explicit formulæ which can result in potentially faster algorithms. Continuing on this note, improving the algorithmic complexity of any of these numerical methods is a persistent problem that has garnered considerable interest from the measurable dynamics community over the last two decades.

On a more theoretical side, it is not yet known if the Frobenius–Perron/Koopman operators are bounded on more general spaces than fractional Sobolev — indeed, there are many more exotic function spaces such as Triebel–Lizorkin, Besov, and Hardy/BMO spaces. These spaces may provide new insights into the spectral properties of these operators. Similarly, wavelets are typically studied in $L^2(\mathbb{X})$ as presented here, however

some theory has been developed for wavelets in $L^1(\mathbb{X})$ and other function spaces, and hence may provide a more general framework than the one presented here. This could allow for new wavelets to be used, and thus giving the user more freedom when selecting a wavelet for the algorithm.

Appendix A

MATLAB Code

A.1 Ulam's method

This code uses the package known as GAIO (Global Analysis of Invariant Objects) to determine the approximation to the transfer operator, \widehat{P} . For more details on GAIO, see [6]. In order to run this code, one must either have the appropriate GAIO files in the same directory or include a line in MATLAB which specifies the directory. This code was based on an example in a presentation [10] by Gary Froyland at the BIRS Workshop on uncovering transport barriers in geophysical flows in September 2013. The slides for this presentation can be found at his website.

```
1 % @title: 2-D Ulam's method for a variation on the
2 % double-gyre.
3 % @author: Hayden Reece Hohns
4 % @date: 16/11/15
5 % @brief: An implementation of Ulam's method on a
6 % variation of the double-gyre flow using GAIO.
7
8 clear all;
9
10 % Parameters for the double-gyre flow.
11 A = 0.25;
12 delta = 0.25;
13 omega = 2 * pi;
14 tStart = 0;
15
16 % Double-Gyre flow
17 v = @(x, T) [-pi * A * x(:, 1) ...
18     .* sin(pi * (delta * sin(omega * T) * x(:, 1) .^ 2 ...
19     + (1 - 2 * delta * sin(omega * T)) * x(:, 1))) ...
20     .* cos(pi * x(:, 2)) ...
21     pi * A * cos(pi * (delta * sin(omega * T) ...
22     * x(:, 1) .^ 2 + (1 - 2 * delta * sin(omega * T)) ...
23     * x(:, 1))) .* sin(pi * x(:, 2)) .* ...
24     (delta * sin(omega * T) * 2 * x(:, 1) ...
25     + (1 - 2 * delta * sin(omega * T)))] ;
26
27 n = 100; % number of steps
```

```
28 h = 0.01; % step size
29 f = @(x) rk4t(v, x, h, n, tStart); % 4th-order Runge-Kutta
30
31 nBox = 50;
32 x = 2 .* linspace(-1 + 1 / (2 * nBox), ...
33 1 - 1 / (2 * nBox), nBox)';
34 y = (1 / 2) .* x;
35 % Create grid with 2-cubes for partitions
36 [XX, YY] = meshgrid(x, y);
37 X = [XX(:, ), YY(:, )]; % nBox by nBox set of vectors
38 c = [1 0.5]; % centre of box
39 r = [1 0.5]; % radius of box
40 t = Tree(c, r); % generate empty tree structure
41 sd = 8; % subdivisions
42 depth = 15; % Depth of tree.
43 % Volume of each box is 2^{-depth}.
44
45 for i = 1:depth, t.set_flags('all', sd);
46 t.subdivide; % make subdivisions in tree structure
47 end
48 boxCollection = t.boxes(-1)'; % box collection
49
50 % Compute/create transition matrix, P has dimension 2^{13}.
51 P = tpmatrix(t, f, X, depth, '0')'; % Given in GAIO
52
53 % Compute left eigenvectors
54 [U_l, V_l] = eigs(P', 3);
55 % Compute (right) eigenvectors
56 [U_r, V_r] = eigs(P, 3);
57
58 figure; % First left eigenvector of U.
59 show2plus(boxCollection, U_l(:, 1))
60 title('First Left Eigenvector'); colorbar;
61
62 figure; % Second left eigenvector of U.
63 show2plus(boxCollection, U_l(:, 2))
64 title('Second Left Eigenvector'); colorbar;
```

A.2 Wavelet threshold for fractional Sobolev norm

Here is some sample code that computes the wavelet fractional Sobolev norm of both the Frobenius–Perron and Koopman eigenvectors. Note the use of a 1-D map solver for Ulam's method in line 16, which constructs the matrix \hat{P} , which defines the 1-step transition matrix.

```
1 % @title: Wavelet Threshold for Mix Norms
2 % @author: Hayden Hohns
3 % @date: 13/10/16
4 % @brief: The wavelet transform can be used to
5 % detect the number of eigenvalues in the isolated
6 % spectrum of an approximation to the transfer and
7 % composition operators, e.g., taken from Ulam's
8 % method or similar.
9
10 clc;
11 clear all;
12
13 numBins = 1000;
14 ptsPerBin = 1000;
15
16 numev = 30; % for spectral picture
17 P = ulam(numBins, ptsPerBin);
18
19 figure;
20 spy(P'); % approximate plot of T
21 xlabel('x_n');
22 ylabel('Tx_n = x_{n+1}');
23
24 [evecR, evalR] = eigs(P, numev, 'LM');
25 [evecL, evalL] = eigs(transpose(P), numev, 'LM');
26 [evecR, evalR] = sortem(evecR, evalR);
27 [evecL, evalL] = sortem(evecR, evalL);
28
29 figure;
30 plot(real(evalR), imag(evalR), 'o', 'MarkerFaceColor', 'b');
31 xlabel('Re \lambda');
32 ylabel('Im \lambda');
33 set(gca, 'fontsize', 18);
34
35 % Plot first five eigenvectors
36 figure;
37 for i = 1 : 5
38     % Plot Koopman (right) eigenvectors
39     subplot(2, 5, i);
40     plot(real(evecR(:, i)));
41     set(gca, 'xtick', []);
42     set(gca, 'ytick', []);
43     % Plot Frobenius-Perron (left) eigenvectors
```

```
44 subplot(2, 5, i + 5);
45 plot(real(evecL(:, i)));
46 set(gca, 'xtick', []);
47 set(gca, 'ytick', []);
48 end
49
50 q = 2; % L^q norm
51 s = 0.4; % smoothing parameter
52 N = numBins;
53
54 maxScale = 600;
55 scales = 1 : maxScale;
56
57 % list of wavelets and markers for final plot
58 wavelets = {'haar', 'db2', 'db8', 'meyr', ...
59 'mexh', 'morl'};
60 markers = {'*', 'o', 'x', '+', '<', '>'};
61
62 sobNormFT = zeros(numev, 1); % Right
63 sobNormWT = zeros(numev, 1); % Left
64 figure;
65
66 for k = 1 : length(wavelets)
67
68     sobNormFT = zeros(numev, 1); % Left
69     waveletName = wavelets{k};
70     marker = markers{k};
71
72     for i = 1 : numev
73
74         l = evecL(:, i); % change for left or right
75         %% Fractional Sobolev norm (Fourier)
76         yL = fftshift(fft(l)); % Left
77         xi = transpose(-N / 2 : N / 2 - 1);
78         zL = yL .* (1 + xi .^ 2) .^ (-s / 2);
79         % remove NaN entry
80         zL(N / 2 + 1) = yL(N / 2 + 1);
81         sobNormFT(i) = norm(ifft(ifftshift(zL)), q);
82
83         %% Fractional Sobolev norm via Wavelet Transform
84         coeffsL = cwt(l, scales, waveletName); % Left
85         energyL = abs(coeffsL) .^ 2;
86         temp = sum(energyL, 2);
87
88         for j = 1 : length(temp)
89
90             sobNormWT(i) = sobNormWT(i) ...
91                 + temp(j) * (2 ^ (2 * j * s));
92
```

```
93         end
94
95     end
96
97     sobNormFT = sobNormFT / max(sobNormFT);
98     sobNormWT = sqrt(sobNormWT);
99     sobNormWT = sobNormWT / max(sobNormWT);
100
101 %% Plotting
102 hold on;
103 plot(sobNormWT, marker, 'MarkerSize', 12);
104 set(gca, 'fontsize', 18);
105
106 sobNormWT = zeros(numev, 1); % Left
107 end
108
109 %% Final Plot
110 hold on;
111 plot(sobNormFT, '^', 'MarkerSize', 12);
112 ylabel('Fractional Sobolev Norm');
113 hh = legend('haar', 'db2', 'db8', 'meyr', 'mexh', ...
114     'morl', 'fft');
115 set(hh, 'FontSize', 18);
```

A.3 Quadruple-gyre Code

Here, a non-linear system of differential equations, commonly referred to as the *quadruple-gyre* is used as a test for the wavelet threshold algorithm.

```
1 % @title: Wavelet threshold for the quadruple-gyre
2 % @author: Hayden Hohns
3 % @date: 31/10/16
4 % @brief: An application of the wavelet fractional
5 % Sobolev norm algorithm for detecting the number
6 % of elements in the isolated spectrum. This
7 % algorithm requires the left and right eigenvectors
8 % of an Ulam or DMD matrix.
9
10 clc;
11 clear all;
12
13 tStart = 0;
14
15 % vector field parameters
16 delta = 0.1;
17 omega = pi / 5;
18 A = 0.1;
19 B = 1;
20
21 % vector field
22 ff = @(t, x) delta * sin(omega * t) .* x .^ 2 ...
23     + (1 - delta * sin(omega * t)) .* x;
24 dff = @(t, x) delta * sin(omega * t) .* x + 1 ...
25     - B * delta * sin(omega * t);
26 g = @(t, x, y) sin(A * pi * ff(t, x)) ...
27     .* cos(B * pi * ff(t, y)) .* dff(t, y);
28 v = @(x, T) [-g(T, x(:, 1), x(:, 2)) ...
29     g(T, x(:, 2), x(:, 1))];
30
31 % n is the number of time steps, h is the step size.
32 n = 100;
33 h = 0.01;
34 % 4th-order Runge-Kutta.
35 f = @(x) rk4t(v, x, h, n, tStart);
36
37 nBox = 50;
38 x = 2 .* linspace(-1 + 1 / (2 * nBox), ...
39     1 - 1 / (2 * nBox), nBox)';
40 y = (1 / 2) .* x;
41 % Create grid with 2-cubes for partitions.
42 [XX, YY] = meshgrid(x, y);
43 X = [XX(:, 1), YY(:, 1)]; % nBox by nBox set of vectors.
44 c = [1 0.5]; % Centre of box.
45 r = [1 0.5]; % Radius of box.
```

```
46 t = Tree(c, r); % Generate empty tree structure.
47 sd = 8; % Subdivisions.
48 depth = 12; % Depth of tree.
49 % Volume of each box is 2^{-depth}.
50
51 for i = 1:depth, t.set_flags('all', sd);
52     % Make subdivisions in tree structure.
53     t.subdivide;
54 end
55 boxCollection = t.boxes(-1)';
56
57 % Compute transition matrix, P has dimension 2^{12}.
58 P = tpmatrix(t, f, X, depth, '0')'; % Given in GAIO
59
60 K = 20;
61 % Compute left eigenvectors
62 [U_l, V_l] = eigs(P', K);
63 % Compute (right) eigenvectors
64 [U_r, V_r] = eigs(P, K);
65
66 % sort eigenvalues and eigenvectors
67 [U_l, V_l] = sortem(U_l, V_l);
68 [U_r, V_r] = sortem(U_r, V_r);
69
70 figure; % First left eigenvector of U.
71 show2plus(boxCollection, U_l(:, 1))
72 title('First Left Eigenvector');
73 colorbar;
74
75 figure; % Second left eigenvector of U.
76 show2plus(boxCollection, U_l(:, 2))
77 title('Second Left Eigenvector');
78 colorbar;
79
80 figure; % Third left eigenvector of U.
81 show2plus(boxCollection, U_l(:, 2))
82 title('Third Left Eigenvector');
83 colorbar;
84
85 figure; % Fourth left eigenvector of U.
86 show2plus(boxCollection, U_l(:, 2))
87 title('Fourth Left Eigenvector');
88 colorbar;
89
90 q = 2; % L^q norm
91 s = 1; % smoothing parameter
92
93 maxScale = 120;
94 scales = 1 : maxScale;
```

```
95 | waveletName = 'sinc';
96 | sobNormWT = zeros(K, 1); % Right
97 | sobNormWTL = sobNormWT; % Left
98 |
99 | for i = 1 : K
100 |
101 |     % i-th right eigenvector
102 |     w = reshape(U_r(:, i), [128, 32]);
103 |     % i-th left eigenvector
104 |     l = reshape(U_l(:, i), [128, 32]);
105 |     [M, N] = size(w);
106 |
107 |     %% Wavelet Fractional Sobolev Norm
108 |     % Right
109 |     coeffsR = cwtft2(w, 'wavelet', waveletName, ...
110 |                         'scales', scales, 'angles', 0);
111 |     energyR = abs(coeffsR.cfs) .^ 2; % from struct
112 |     temp1 = sum(energyR, 2);
113 |     temp2 = sum(temp1, 3);
114 |     [cols, rows] = size(temp2);
115 |
116 |     for j = 1 : cols
117 |         for k = 1 : rows
118 |             sobNormWT(i) = sobNormWT(i) ...
119 |                             + temp2(j, k) * 2 ^ (-j * k * s);
120 |         end
121 |     end
122 |
123 |     % Left
124 |     coeffsL = cwtft2(l, 'wavelet', waveletName, ...
125 |                         'scales', scales, 'angles', 0);
126 |     energyL = abs(coeffsL.cfs) .^ 2; % from struct
127 |     temp1 = sum(energyL, 2);
128 |     temp2 = sum(temp1, 3);
129 |     [cols, rows] = size(temp2);
130 |
131 |     for j = 1 : cols
132 |         for k = 1 : rows
133 |             sobNormWTL(i) = sobNormWTL(i) ...
134 |                             + temp2(j, k) * 2 ^ (-j * k * s);
135 |         end
136 |     end
137 |
138 | end
139 |
140 | sobNormWT = sobNormWT / max(sobNormWT);
141 | sobNormWTL = sobNormWTL / max(sobNormWTL);
142 |
143 | %% Plotting
```

```
144 figure;
145 plot(sobNormWT, '*', 'MarkerSize', 12);
146 xlabel('Right eigenvectors');
147 ylabel('Fractional Sobolev Norm');
148
149 figure;
150 plot(sobNormWTL, '*', 'MarkerSize', 12);
151 xlabel('Left eigenvectors');
152 ylabel('Fractional Sobolev Norm');
```

Bibliography

- [1] J. AARONSON, *An Introduction to Infinite Ergodic Theory*, vol. 50 of Mathematical Surveys and Monographs, American Mathematical Society, 1997.
- [2] V. BALADI, *Positive Transfer Operators an Decay of Correlations*, World Scientific, River Edge, NJ, 2000.
- [3] V. BALADI AND S. GOUËZEL, *Good Banach spaces for piecewise hyperbolic maps via interpolation*, Annales De L Institut Henri Poincaré Analyse De Non Linéaire, (2009), pp. 1453–1481.
- [4] E. M. BOLLT AND N. SANTITISSADEEKORN, *Applied and Computational Measurable Dynamics*, Society for Industrial and Applied Mathematics, 2013.
- [5] I. DAUBECHIES, *Ten lectures on wavelets*, vol. 61 of CBMS-NSF Regional Conference Series in Applied Mathematics, Society for Industrial and Applied Mathematics, 1992.
- [6] M. DELLNITZ, G. FROYLAND, AND O. JUNGE, *The algorithms behind GAI - Set oriented numerical methods for dynamical systems*, in Ergodic theory, analysis, analysis, and efficient simulation of dynamical systems, Springer, 2000, pp. 145–174.
- [7] M. DELLNITZ, G. FROYLAND, AND S. SERTL, *On the isolated spectrum of the Perron-Frobenius operator*, Nonlinearity, 13 (2000), pp. 1171–1188.
- [8] A. DENNER, O. JUNGE, AND D. MATTHES, *Computing Coherent Sets using the Fokker-Planck Equation*. Pre-print, 2016.
- [9] J. DING AND A. ZHOU, *Finite approximations of Frobenius-Perron operators. A solution of Ulam's conjecture on multi-dimensional transformations.*, Physica D, 92 (1996), pp. 61–68.
- [10] G. FROYLAND, *A tutorial on transfer operator methods for numerical analysis of dynamical systems*. Presented at the BIRS Workshop on Uncovering transport barriers in geophysical flows, September 2013.
- [11] G. FROYLAND, C. GONZÁLEZ-TOKMAN, AND A. QUAS, *Detecting isolated spectrum of transfer and Koopman operators with Fourier analytic tools*, Journal of Computational Dynamics, 1 (2014), pp. 249–278.
- [12] P. R. HALMOS, *Lectures on ergodic theory*, vol. 142, American Mathematical Society, 1956.
- [13] O. JUNGE AND P. KOLTAI, *Discretization of transfer operators using a sparse hierarchical tensor basis – the Sparse Ulam method*, SIAM Journal on Numerical Analysis, 47 (2009), pp. 3464–3485.

BIBLIOGRAPHY

- [14] G. KELLER AND C. LIVERANI, *Stability of the spectrum for transfer operators*, Ann. Scuola Norm. Sup. Pisa Cl. Sci., 4 (1999), pp. 141–152.
- [15] S. KLUS, P. KOLTAI, AND C. SCHÜTTE, *On the numerical approximation of the Perron-Frobenius and Koopman operator*, Journal of Computational Dynamics, 3 (2016), pp. 51–79.
- [16] A. LASOTA AND M. C. MACKEY, *Chaos, Fractals, and Noise: Stochastic Aspects of Dynamics*, vol. 97 of Applied Mathematical Sciences, Springer-Verlag New York, 2 ed., 1994.
- [17] T.-Y. LI, *Finite approximation for the Frobenius-Perron operator. A solution to Ulam's conjecture*, Journal of Approximation Theory, 17 (1976), pp. 177–186.
- [18] S. MALLAT, *A Wavelet Tour of Signal Processing, Third Edition: The Sparse Way*, Academic Press, 2009.
- [19] Y. MEYER, *Wavelets and Operators: Advanced Mathematics*, Cambridge University Press, 1992.
- [20] R. MURRAY, *Discrete approximation of invariant densities*, PhD thesis, University of Cambridge, 1997.
- [21] M. PINSKY, *Introduction to Fourier Analysis and Wavelets*, vol. 102 of Graduate Studies in Mathematics, American Mathematical Society, 2009.
- [22] B. SIMON, *Harmonic Analysis: A Comprehensive Course in Analysis, Part 3*, American Mathematical Society, 2015.
- [23] ——, *Real Analysis: A Comprehensive Course in Analysis, Part 1*, American Mathematical Society, 2015.
- [24] J.-L. THIFFEAULT, *Using multiscale norms to quantify mixing and transport*, Nonlinearity, 25 (2012).
- [25] S. M. ULAM, *A Collection of Mathematical Problems*, Interscience Publisher NY, (1960).
- [26] M. VIANA AND K. OLIVEIRA, *Foundations of Ergodic Theory*, vol. 151, Cambridge University Press, 2016.